UiT The Arctic University of Norway

Faculty of Sciences and Technology

Department of Geosciences

Newly found evidence of the Late Devonian extinction by microtektites in black shales: Sellersburg, Indiana, USA

Emiliyan Nedelchev

Master's thesis in Geology GEO-3900 May 2024

Abstract

Our planet has experienced at least five major mass extinction events, which have occasionally brought the flora and fauna to almost complete collapse, yet they have been pivotal in the evolution of life as we know it. This thesis explores potential causes of mass extinctions, focusing particularly on the Late Devonian mass extinction event, which is the least understood of the major five. Over the span of the early Paleozoic and the Devonian, the planet experienced extensive plate tectonic reorganization which resulted in the formation major orogenic belts, extensive rifting and seafloor spreading, as well as associated volcanism related to the emplacement of large igneous provinces (LIPs). Collectively, these tectonic changes drove the development of various sedimentary basins in the Devonian, including a series of foreland and intracratonic basins to form on Laurentia (i.e., present day North America). The Illinois Basin is one such intracratonic basin, which host a thick sedimentary succession, including Devonian strata. The mudstone-dominated Devonian part of basin fill, which was deposited in a shallow and partly restricted marine basin, holds the potential of harboring evidence of one of many drivers, which over the period of some few million years, triggered the Late Devonian mass extinction. By combining conventional petrographic analysis of some black shale samples (from the Late Devonian-aged New Albany Shale group) with X-Ray Fluorescence (XRF), X-Ray Diffraction (XRD), and Scanning Electron Microscopy (SEM) analyses, this study investigate microscopic spherules, known as microtektites, which is thought to be dust-sized impact ejecta debris that settled from the atmosphere into this vast basin following a potential lethal meteor impact somewhere else on the planet. . Across the planet, multiple Devonian-aged impacts are known, especially from near or at the Frasnian – Famennian boundary (c. 372.2 Ma), which thus could be the source of these microtektites. The investigated, finely laminated black shales from the Illinois Basin also contain abundant pyrite framboids, recording the anoxic conditions that prevailed in the basin at the time of deposition. Similar black shales of Late Devonian age occur elsewhere on the planet, suggesting that widespread anoxia could be an important factor leading to the mass extinction. Indeed, the scientific community have hitherto, not fully agreed on the key causal factor that drove the Late Devonian extinction event, although volcanic activity related to LIPs, widespread oceanic anoxia, onset of severe glaciations, as well as vascular plant migration on land has variably been proposed as the main drivers. Due to limited number of locations having preserved Late Devonian-aged

microtektites, the impact hypothesis is rarely mentioned as a potential cause. Therefore, this thesis aims to rejuvenate the bolide impact-theory, which may have influenced and substantially changed the course of the Late Devonian biotic evolution, or the very least contributed to the environmental crisis that was already gripping the Late Devonian World.

DEDICATION

This thesis is being dedicated in memory of late Dr. Glenn Mason, Professor of Geosciences at Indiana University Southeast. He was a mentor and a friend who never seized to believe in my perseverance. For that I will forever be grateful.

Acknowledgements

I would like to express my sincere gratitude of having Sten-Andreas Grundvåg as a supervisor, helping me along the way with feedback and guidance and taking me under his wing as a master student.

I would also like to thank Senior Engineer Trine Merete Dahl and Head Engineer Karina Monsen for guiding me on using the equipment provided by the Geology Lab at UiT and Jiri Konopasek for showing me a method of picking magnetic particles, which was crucial in the preparation of samples.

Contents

1 Introduction

Throughout Earth's history the planet has endured multiple mass extinction events, including several which brought the flora and fauna to almost complete collapse (Elewa et al., 2019; Marshall, 2023). There are five well known and widely documented major mass extinctions of global proportions, the first occurred at the end of the Ordovician, followed by the Late Devonian, the end Permian, the Triassic–Jurassic, and lastly the Cretaceous–Paleogene mass extinctions (e.g., Fig. 1.1; Elewa et al., 2019).

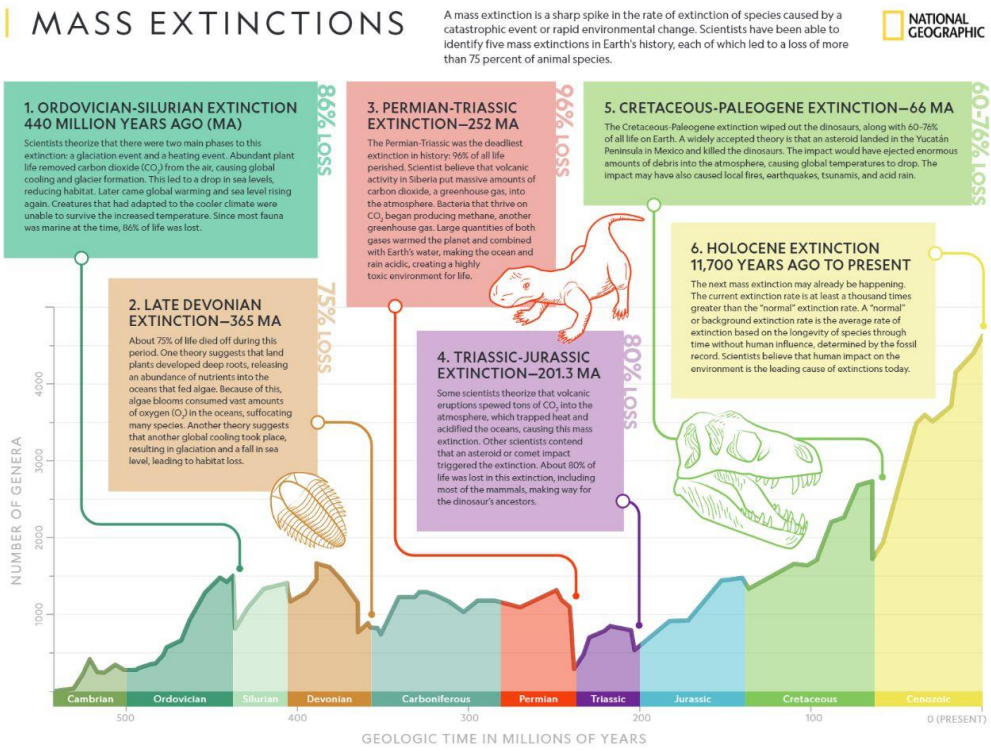

Fig. 1.1 *Extinction overview summarizing causes, loss of life (National Geographic)*

Present day plant and animal species are thus based on the evolution of small pools of surviving ancestors that were able to successively overcome the unfavorable conditions brought by these global catastrophes. What defines each of these mass extinctions, is the rapid loss of living organisms caused by catastrophic events such as widespread volcanism, commonly associated with the emplacement of large igneous provinces (LIPs), global anoxia, meteor impacts, or rapid deterioration of the global climate (Algeo et al., 2023; Arndt et al., 2011). Most of the five great extinctions that have occurred on this planet have been studied widely. The Cretaceous–Paleogene mass extinction is perhaps the most famous event due to the loss of most

dinosaur species following a meteor impact on the Yucatán Peninsula in the Gulf of Mexico 66 million years ago (Chiarenza et al., 2020). It has also been suggested that volcanism and global anoxia contributed to the extinction event, although there is consensus that the meteor impact, which created the renown 180 km wide Chicxulub crater, was the key causal factor (Keller et al., 2009; Arndt et al., 2011; Chiarenza et al., 2020; Hallam, 2022). The cause of the much older Late Devonian mass extinction event has for long been debated (McGhee et al., 2021). Rakocinski et al. (2020), for example, have proposed that a chain of magmatic events promoted global anoxia by the introduction of high quantity of mercury (Hg) along with the influx of fine-grained sediments into the oceans. Global oceanic anoxia has also been considered as a causal factor, but the fact that there are only a handful of reported locations of marine sedimentary strata recording such conditions in South China (Zhang et al., 2020) and central Europe (Bond et al.,2004), begs the question whether anoxia was really that widespread and thus affecting the Late Devonian oceans. In addition, other proposed drivers include substantial sea level changes, and the possible onset of severe icehouse conditions related to the Late Paleozoic Ice Age which possibly was initiated during the late Famennian (McGhee et al., 2021; Barash, 2017; Barash, 2016). Moreover, McGhee (2001) have suggested that during the time of the Frasnian–Famennian boundary interval (c. 372.2 Ma), the planet may have been hit by a comet or an asteroid that may have broken up on its way to Earth and consequently caused multiple impacts possibly recorded by the Alamo impact crater in Nevada, the Siljan Ring in Sweden, and the Flynn Creek crater in Tennessee, USA. Whatever cause, Elewa et al. (2019), suggested that the Late Devonian mass extinction was the culmination of multiple contemporaneous events that collectively caused one of the bigger known taxa losses with about 70% to 82% of all species vanishing. Another estimate by Claeys et al. (1992), suggest that the mass extinction heavily affected reefal organisms, corals, stromatoporoids, tentaculids, and brachiopods, together accounting for a loss of 21% of all families, 50% of all genera, and a total species loss of 70%.

In contrast to the other mass extinction events, there have not been established a definitive timeframe for the Late Devonian extinction event. However, it is believed that the main phase occurred around the time of the Frasnian–Famennian boundary interval (c. 372.2 Ma), culminating in what is known as the Hangenberg Event at the end of the Famennian stage (c. 358.9 Ma). As such, it appears that the Late Devonian mass extinction encompass several shorter superimposed events spanning several million years (e.g., Claeys et al., 1992) rather

than a single event. It thus includes the so-called Lower and Upper Kellwasser anoxic events in the late Frasnian, which is associated with horizons of black shale in Europe, North America, and China (e.g., Bond et al., 2013), as well as the Hagenberg anoxic event in the latest Famennian (referred to as the Devonian extinction in some literature), the latter possibly being a global event (Kaiser et al., 2016). Hence, it appears that global oceanic anoxia may have played a key role in the decimation of life during the Late Devonian period (e.g., Kaiser et al., 2016; Zhang et al., 2020). Another idea is that Earth was subject to a multi pulse meteor impact around the time of the Frasnian–Famennian boundary, which may have caused severe climatic changes that lasted for several million years eventually culminating in a mass extinction (Barash, 2016; McGhee et al., 2021). However, since there are few localities on Earth with preserved Late Devonian impact debris or craters that would suggest one or several bolide impacts at the time of the known extinction events in the Frasnian and Famennian, many in the scientific community tend to ignore or exclude the multiple impact hypothesis.

Craters and impact debris are not the only indicators of major impacts. Other proxies in the sedimentary record includes the presence of shocked quartz (i.e., coesite) and Iridium (Ir) enrichment in distinct sediment horizons, as is the case for the Cretaceous–Paleogene boundary layer, which has been directly linked to the impact creating the Chicxulub crater (Keller et al., 2009; Hallam, 2022). A less known and used proxy is the presence of impact ejecta, particularly so-called microtektites (Claeys et al., 1992; Barash, 2016).

Earth is constantly bombarded by smaller and larger meteors, most which burns up and do not survive a trip through the atmosphere. However, when our planet is struck by a cosmic body, or meteorites, of proportions large enough to escape the atmospheric entry, an impact occur. During entry of such projectiles into Earth's atmosphere, portions of its mass burns from the friction and melt in the process, which may result in precipitation of micro-scale molten droplets (Lyne et al., 1996). Everything else that has survived the entry friction and associate heat eventually comes to a full impact when hitting the planet's surface. At the time of the impact, given that the meteorite is of a certain size, a crater is formed and enormous load of sediment and/or bedrock, depending on the geology at the impact location, is being violently deformed and abruptly displaced by the immense force of the impact. All displaced material which has been exhumed, is given the name impact ejecta (e.g. Richardson et al., 2006). Like the size classification of sediments, ejecta ranges from extremely large lumps of land/rock that are thrown into the air all the way down to microscopic pieces that can be widely distributed,

potentially worldwide. Less dense, dust-like ejecta may find itself in or above the atmosphere where it may linger there for years to come before these fine-grained particles settle to the surface of the Earth in the form of silica rich microscopic spherules referred to as microtektites (or sometimes micro-meteorites; e.g. Chernonozhkin et al., 2021; Lorenz, 2000). On some occasions these can be globally distributed resulting in the wide-spread deposition of fine dust that represent leftovers from an impact which may have happened several decades or more prior. Intriguingly, microtektites have been reported from Upper Devonian shales in both the Dinant Basin in Belgium and Qidong in China (Claeys & Casier, 1994). Thus, could it be that impacts by one or several large cosmic bodies may have triggered or contributed to the Late Devonian mass extinction event as previously suggested by McGhee (2001)? However, there are few proposed craters that may be the source of the microtektites at the reported localities. Mikheeva (2022) suggests a crater diameter of at least 50 km for cataclysmic conditions to occur and cause an extinction. According to Claeys et al. (1992), the spheroids documented in Belgium may be the result of the Siljan Ring in Sweden, a crater structure with a diameter of 52 km and an age of c. 368±1 Ma (i.e. early to middle Famennian). For the extinction at the Frasnian–Famennian boundary, Mikheeva (2022) proposed seven potential structures, with the Siljan Ring, as well as the Woodleigh and the Alamo craters, in Australia and the USA, respectively, being the best contenders followed by the Taihu lake crater in China and some very large, yet speculative/unproven craters in Russia.

When the suggested craters are taken under consideration as the likely source of the microtektites in Belgium and China, one must ask whether it is possible to find similar-aged micro-debris anywhere else on the planet? According to Alvarez (1994), distribution of impact related particles is affected by the rotational forces of the planet. Thus, with the help of the planet's rotation around its own axis, atmospheric conditions, and the Coriolis effect, fine-grained impact ejecta has the potential to spread across the entirety of the planet's surface given sufficient time and the right conditions (Glass & Simonson, 2012). By taking into consideration the planet's eastern spin around its axis, airborne microscopic dust will indeed have a westward direction on the northern hemisphere, possibly without changing its latitude over time. The opposite effect occurs if the impact is located on the southern hemisphere. Moreover, if the Coriolis force is considered, as well as the Late Devonian plate tectonics (Fig. 1.2), a potential relationship between the microtektites in Belgium and China emerges, both basins being positioned in the same microtektite depositional belt.

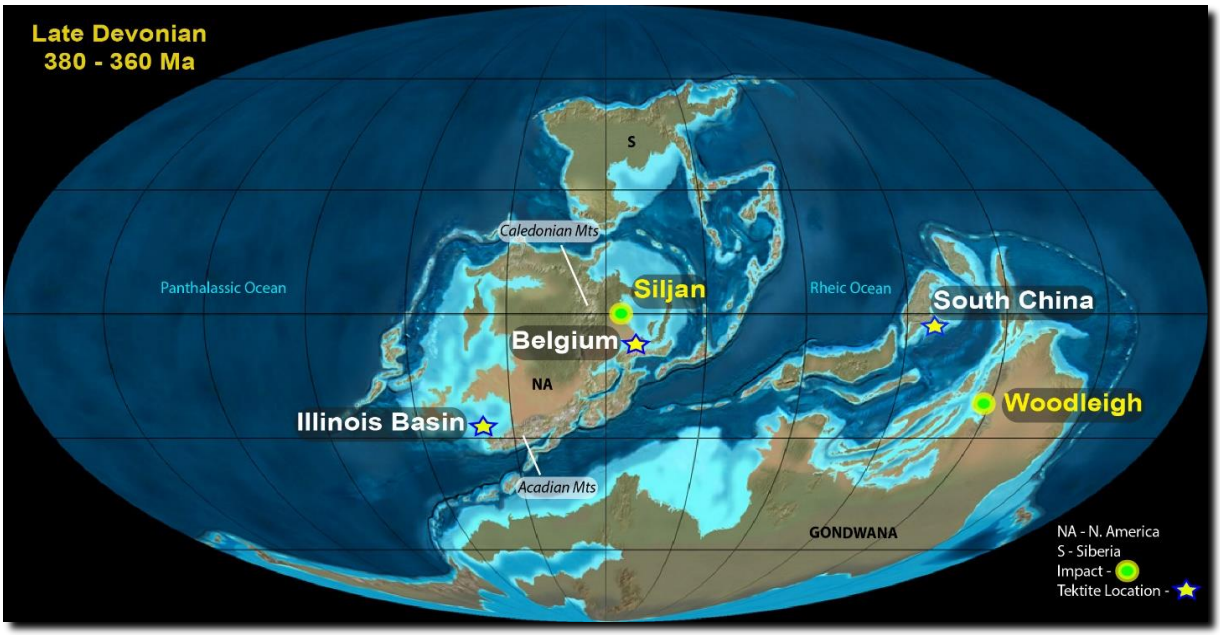

Fig. 1.2 *Late Devonian map visualizing localities where tektites are found and crater locations. Intriguingly they all line up in a belt spanning the same paleo-latitudes (©Ron Blakey, NAU Geology) (edited by E. N.).*

Could other sedimentary basins within this proposed belt also contain evidence of Late Devonian impact ejecta in the shape of microtektites and associated particles? Maybe. One basin holding the potential to unravel the presence and origin of Late Devonian microtektites is the Illinois Basin in North America (Fig. 1.2). During the Late Devonian, the interior of North America was part of Laurentia and hosted several marine basins which could have acted as sinks for fine-grained impact-related dust (Fig. 1.2). The basin contains a thick succession of weakly radioactive, pyrite-bearing black shale of Late Devonian age (e.g., Anderson et al., 1987; Ramirez et al., 2023), lithostratigraphically assigned to the New Albany Shale Group, which reportedly exhibit various micro-scale spheres (Mason et al., 2016). This study thus set out to explore the origin of the spheres in the Illinois Basin, aiming to establish whether they are microtektites that can be linked to a potential meteorite impact that promoted the Late Devonian mass extinction event. As such, this thesis aims to shed new light on the occurrence and origin of Late Devonian microtektites, supplementing previous studies elsewhere but also potentially expanding the area of distribution to demonstrate their global significance. If the spheres found within the black shale beds of the Illinois Basin are indeed of impact origin, this could cause shockwaves through the scientific community that explores the prospects of impact related events during the Frasnian–Famennian boundary interval. A new microtektite horizon

will most certainly rejuvenate the search for answers as to what was the leading cause of the extinction. The research questions this thesis will try to answer are as follows:

- What does the spheres in the New Albany Shale Group of the Illinois Basin consist of?
- Do the spheres vary in shape and size, and what can be the cause for such variations?
- Can the composition, size and shape of the spheres unravel their origin?
- Are there any alternative and competing interpretations apart from an impact origin that offer viable explanations for the occurrence of the spheres?

2 Impact ejecta theory and microtektites

Glass and Simonson (2012) highlighted the importance of studying impact debris classifying ejecta by size and composition based on the distance traveled of ejected particles from the impact epicenter. There are two main types of ejecta classification based on: 1) distance from the epicenter, and 2) composition and shape of the ejecta. The first define ejecta by distance from the crater and encompass proximal and distal ejecta (Fig. 2.1). Proximal ejecta typically occurs within less than 2.5 times the crater diameter, whereas distal ejecta is in an area of more than 2.5 times the crater diameter.

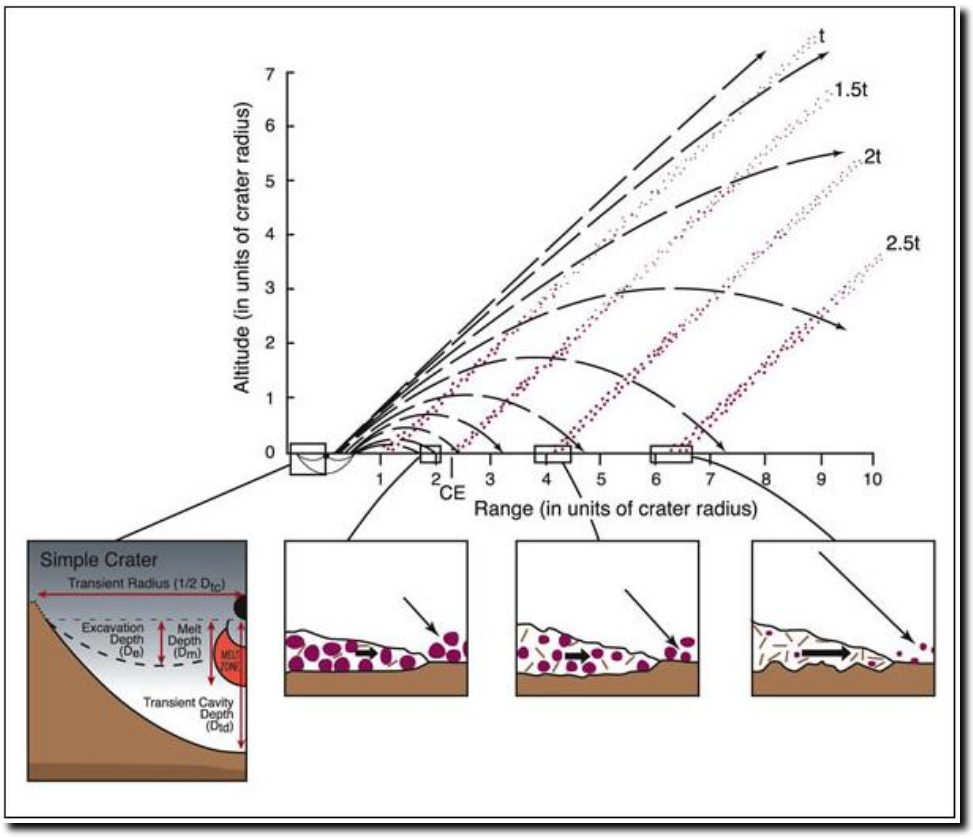

Fig. 2.1 *Representation of ejection debris distribution post impact. From Richardson et al. (2006).*

Proximal ejecta therefore includes anything from exhumed land/rock and large slabs down to detritus a few cm wide, whereas distal ejecta typically ranges from 1 cm to 1 mm. Distal particles of this size are considered tektites whereas anything less than that is classified as microtektites. When size, composition and shape of the smallest distal ejecta is taken into consideration, microtektites appears to come in two types: 1) 1 mm–400 µm wide spheres mostly made of glass (i.e., felsic), and 2) so-called microkrystites, which are particles <400 µm wide and which contain impurities injected by the colliding body, so they tend to be darker in color (more mafic). Both types of microtektites are defined by characteristics that are unique which makes them very easily identifiable (Fig. 2.2).

Fig. 2.2 *Variety of tektites (From Pillans et al. 2012)*

For instance, they exhibit many shapes like discs, teardrops, dumbbells, and spheres. These forms are made by the rotation of the particle during flight in the atmosphere, and others like the discs, are made due to compaction during burial. Surface features like vesicles, grooves, and striations can be observed on some grains, recording air friction, and escaping of gases from within. According to Glass and Simonson (2012), microkrystites, formed during the late Eocene contain clinopyroxene minerals along with Iridium (Ir) and Nickel (Ni) elements commonly found in high amounts in meteorites compared to what is naturally occurring in the Earth crust. Additionally, Chromium (Cr) and Cobalt (Co) enrichment is common. In contrast, microtektite particles only appear as spheres. Along with tektites, shock metamorphism is also a good indication of an impact. Planar deformation features (PDFs), sometimes referred to as shock lamellae, are alterations in mineral's crystallography which appears as fractures in various directions due to the immense pressure induced from an impact. Depending on the location and geological setting, if the bedrock is rich in carbon, a type of diamond can be formed during shock metamorphism called Lonsdaleite. In addition, shocked quartz (i.e. coesite or lechatelierite) have been reported in many impact craters. Furthermore, Glass and Simonson

(2012), argue that the composition of tektites varies from location to location by comparing ejecta from various craters of Paleozoic, Mesozoic, and Cenozoic ages from different areas. For example, Cenozoic tektites which occur in strewn fields (i.e. an area rich in meteorites from a single impact) in Australia and Indonesia, the Ivory Coast of Africa, and North America with ages as old as 35 Ma. When seen separately, tektites from each location seem homogenous, but when looked in a bulk, obvious difference in source rock can be observed. A good example is a layer of microkrystites from the late Eocene, which are rich in clinopyroxene minerals typical for rocks of metamorphic origin and are not associated with the depositional environments of the hosting sedimentary rocks. On rare occasions a mineral replacement may take place by substituting the sphere contents with various clay minerals or pyrite. Many of the reported Eocene particles are low on silica and aluminum oxides, but are rich on Cr, Co, Ni and Ir. Signs of shock metamorphism along with the elemental composition suggest these grains were formed by the cosmic body itself. Late Cretaceous microtektites can be found in a 5000 km radius from their associated impact crater in Mexico, where microkrystites are seen worldwide (Glass & Simonson, 2012). Late Triassic tektites are found in England and are believed to be derived from an impact called Manicouagan (Clutson et al. 2018). There is a possibility of microtektites to be replaced by other minerals during burial and diagenesis, while microkrystites tend to keep their original composition. The Late Devonian microtektites documented in Belgium and China are similar in composition to the Cenozoic microtektites described by Glass and Simonson (2012), although no Ir enrichment have been demonstrated nor any signs of shock metamorphism observed or reported.

The spheroids reported in the Late Devonian of Belgium are found in a black shale deposit, rich on organic matter and pyrite (e.g. Claeys et al. 1992). These tektites range from 1 mm to 50 µm with average size of 300 µm. Most of the spheres are reportedly yellow to transparent (i.e., felsic microtektites), and some are dark metallic (i.e., mafic microkrystite). Well rounded, elongated with teardrop and dumbbell shapes along with some fusing is common expressions. Broken fragments apparently resemble flaking obsidian by having conchoidal fractures. Surface morphology includes well preserved smooth glassy textures or more abnormal topographies. Some investigators may thus easily mistake the spheres for a volcanic byproduct, but to qualify for volcanic in nature, clearly visible phenocrysts (large crystal within matrix) must be present (Claeys et al. 1992). One notable feature of the Late Devonian microtektites is that the spheres are well preserved despite their age and their general low

resistance to weathering. Usually, over time, glass becomes unstable and loses its clear transparent appearance and forms other crystals within, whereas after 365 ± 5 Ma, spheres have no devitrification. This preservation may be attributed due to the low water content of 0.009% H_2O in the tektites along with rapid burial aided by fine grained silica rich sediment (Claeys et al. 1992, 1994). Once in situ and sediment has turned into shale during burial, compaction and diagenesis, the rock becomes like a time capsule with its low porosity and permeability restricting water from reaching the spherules. Preservation at the Hony location in Belgium is very good because of a carbonate or clay mineral coating acting as a shield against weathering (Claeys & Casier, 1994). According to Claeys et al. (1992), the tektites in Belgium are made of five main elements which are: Potassium (K), Aluminum (Al), Iron (Fe), Silicon (Si) and Calcium (Ca), whereas Sulfur (S) can be found in minor quantities. There is a high K_2O/Na_2O ratio and high $[Al_2O_3 + (K_2O + Na_2O)]$ ratios, which are typically seen in tektites elsewhere like the Cenozoic tektites (Claeys & Casier, 1994).

Claeys et al. (1992) reports that the microtektites found in China share similar characteristics as their Belgian counterpart, all being rich in K and Si. The only difference is that the Qidong microtektites in China exhibit Ir traces. But according to Barash (2016), the highly speculative Ir anomaly documented in China may not be due to an impact, but instead be the biproduct of a cyanobacteria called *Frutexites*. Some parts of the bacteria can concentrate elements such as Manganese (Mn), Platinum (Pt), Iron (Fe), Cobalt (Co), Arsenic (As) as well as Ir, thus explaining the higher than usual levels found at that location.

3 Local geologic setting

3.1 Global plate tectonics during the early Paleozoic to latest Devonian

During the Late Devonian, the planet's land distribution was divided into two major landmasses, the supercontinent of Gondwana on the southern hemisphere, and the minor supercontinent of Laurussia on the northern hemisphere (e.g., Golonka, 2020; Fig. 3.1). The study area and basin investigated in this study was part of Laurussia throughout the Devonian. The formation of Laurussia was initiated by the closure of the Iapetus Ocean and the following head-on collision of major continental masses like Laurentia and Baltica, as well as island arcs and micro continents, such as Avalonia, together forming a prominent orogenic belt stretching more than 3000 km (Murphy et al. 1999), including the so-called Acadian and the Caledonian orogens (e.g. Corfu et al. 2015). The connection between the two orogenic belts from north to south can be seen in similar grade and style of metamorphic facies, stacks of allochthons, as well as a series of partly connected post-orogenic basins of Devonian age spanning 4500 km, which hosts the well-known Old Red Sandstone succession (Torsvik et al. 2005). Remnants of this ancient mountain chain are visible today as the Appalachian Mountains in North America and the Caledonian mountains of northwestern Europe, including western Norway, and East Greenland on the adjacent coastline of the Atlantic Ocean.

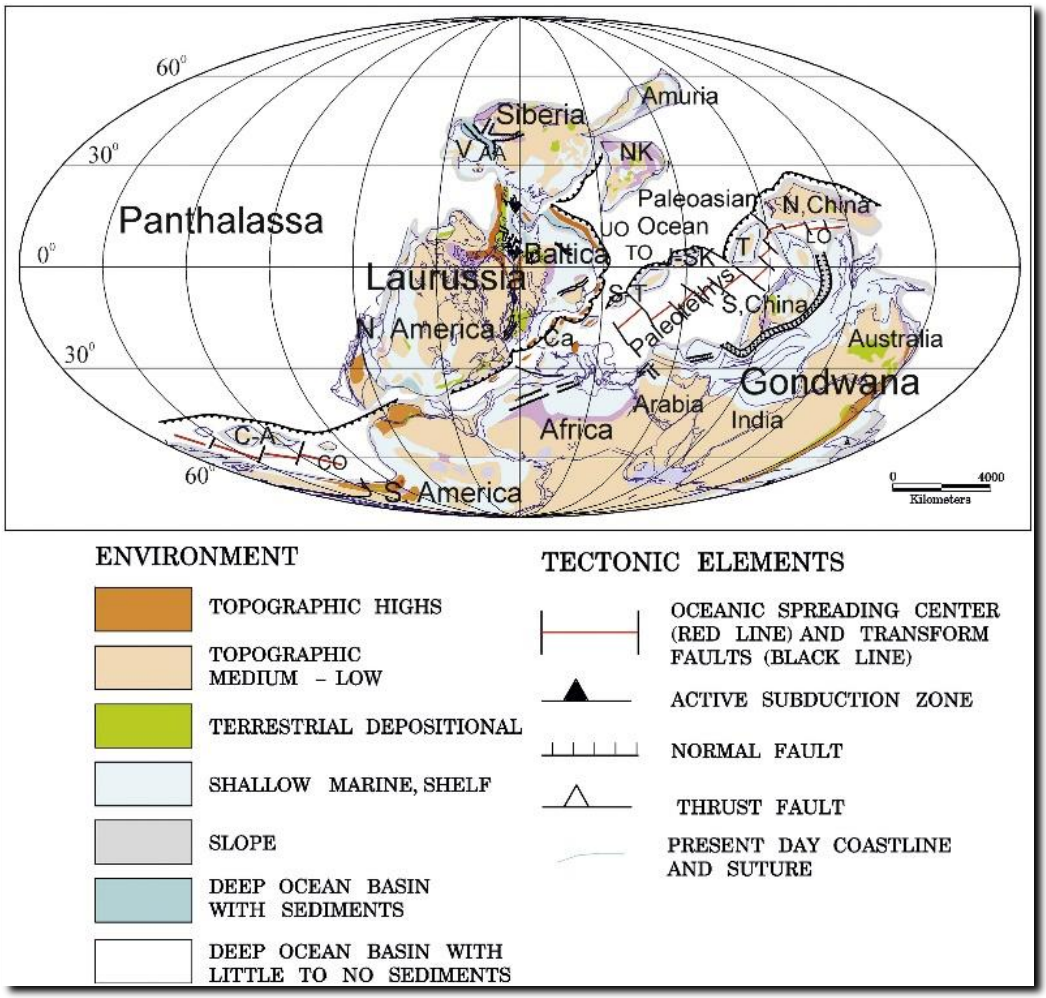

Fig. 3.1 *Representation of land distribution during the late Devonian 370 Ma. From Golonka (2020).*

The Iapetus Ocean formed in the Neoproterozoic and was surrounded by Baltica, Avalonia and Laurentia in the Early Ordovician (Golonka et al. 2023). The Ordovician period was dominated by intense magmatism and subduction zones. Avalonia and Ganderia terranes were advancing to Laurentia, while closing in on the Iapetus Ocean (Meinhold et al. 2011). The break-up and drifting of Avalonia caused the formation of the Rheic Ocean. At this time, an already subsiding terrane, called Gander, had already collided with Laurentia before Avalonia accreted onto, and subsequently, subducted underneath the eastern margin of Laurentia. This chain of events resulted in the creation of a magmatic zone along the Salinic mountains which spawn a volcanic arc (Domier et al. 2014; Fig. 3.2).

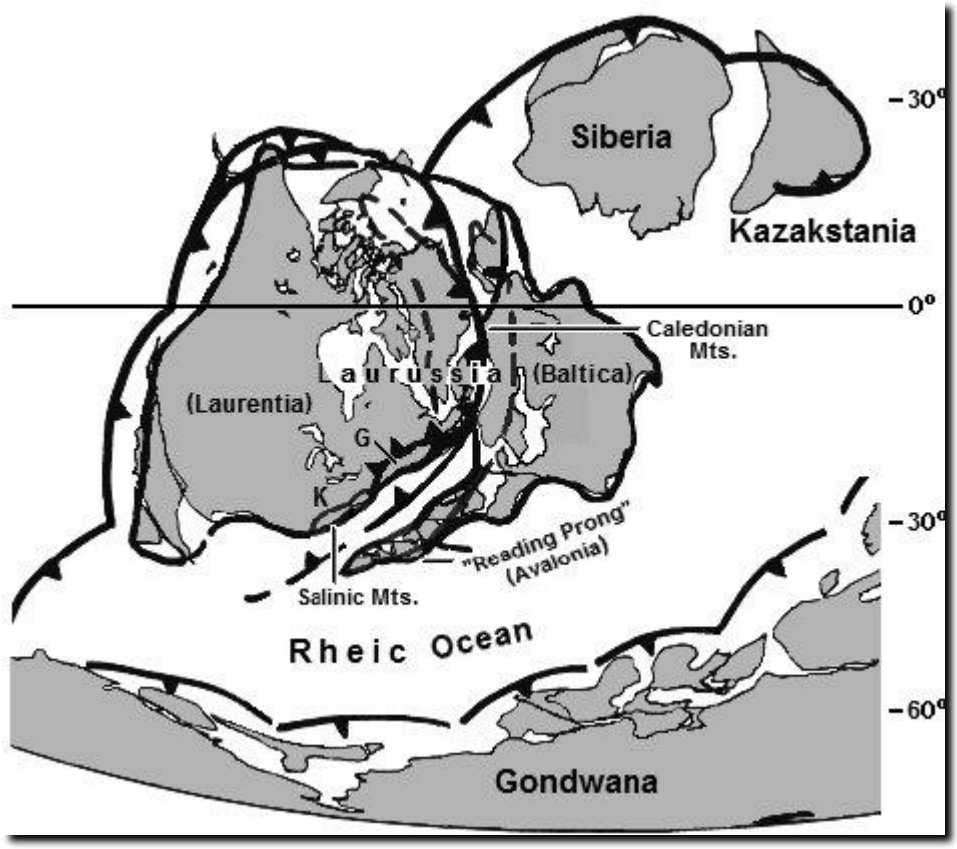

Fig. 3.2 *Early Silurian showing Salinic mountains (pre-Acadian orogeny) adjacent to Kentucky (K). Salinic mountains are the product of Gander subduction. From Ettensohn et al. (2013).*

In the Late Ordovician to early Silurian (i.e. the Llandovery), Baltica began to close in on Laurentia. In the process, the Tornquist oceanic plate (Fig. 3.3) adjacent to Baltica to the south began to subduct under northern Avalonia. As this happened, the rest of Avalonia was slowly pushed into the eastern margin of Laurentia, while portion of Ganderia, which had collided earlier, started to be subducted (Jutras and Dostal, 2023).

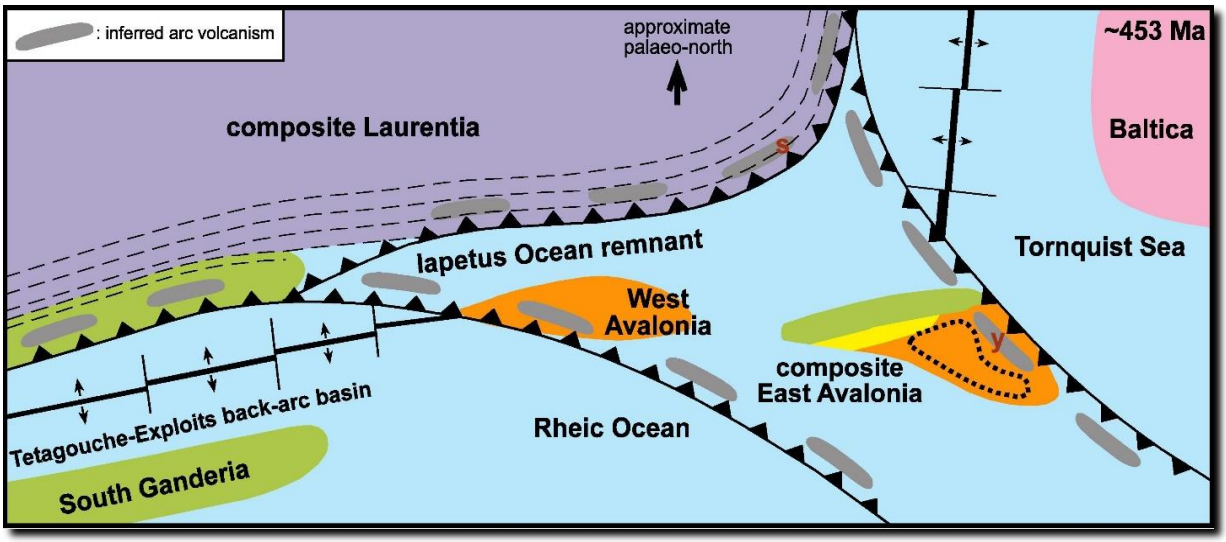

Fig 3.3 *Shows Late Ordovician to early Silurian distribution of terranes in proximity before the formation of Laurasia. From Jutras and Dostal (2023).*

During early Silurian, the paleo-continents of Laurentia and Baltica along with the micro-continent of Avalonia collided into each other because of convergence caused by mantle plume dynamics, eventually leading to the closure of the Iapetus Ocean and the formation of a major, supra-regional continent-continent collision zone (Domier et al., 2014; Golonka, 2020). The resulting closure and collision thus drove the formation of the Caledonian orogenic belt and its southward continuation, the Acadian orogen, unifying the various cratons forming Laurussia, commonly referred to as the Old Red Sandstone Continent. The collision and mountain-building event continued through the Devonian. During the late Silurian to Early Devonian (423–416 Ma), the bulk of subduction of Avalonia occurred, although it never became fully subducted. However, the subduction-induced sinking resumed in the Middle to Late Devonian, when the so-called Meguma terrane collided with the eastern side of the accreted part of Avalonia around 360 Ma, causing the formation of the Neo-Acadian orogeny (Domier et. al., 2014; Golonka, 2020). The Acadian orogeny is thought to have lasted between 460–370 Ma, with a likely driver for its uplift being the movement of Laurussia over a mantle plume which allowed it to be sourced with intrusions of granitic composition, along with the melting of crustal rocks from Avalonia and Meguma during active volcanism (Fig. 3.4) including some accretional buildup. Present day Newfoundland is predominantly made of Avalonian and Megumaian sourced rocks. (Cocks and Torsvik, 2011). An extensional phase during the Late Devonian resulted in the creation of Paleotethys Ocean with rifting between Gondwana and

China. Southeastern side of Laurussia is not affected in a major way during the rifting stage, Golonka 2020, (Fig. 3.4).

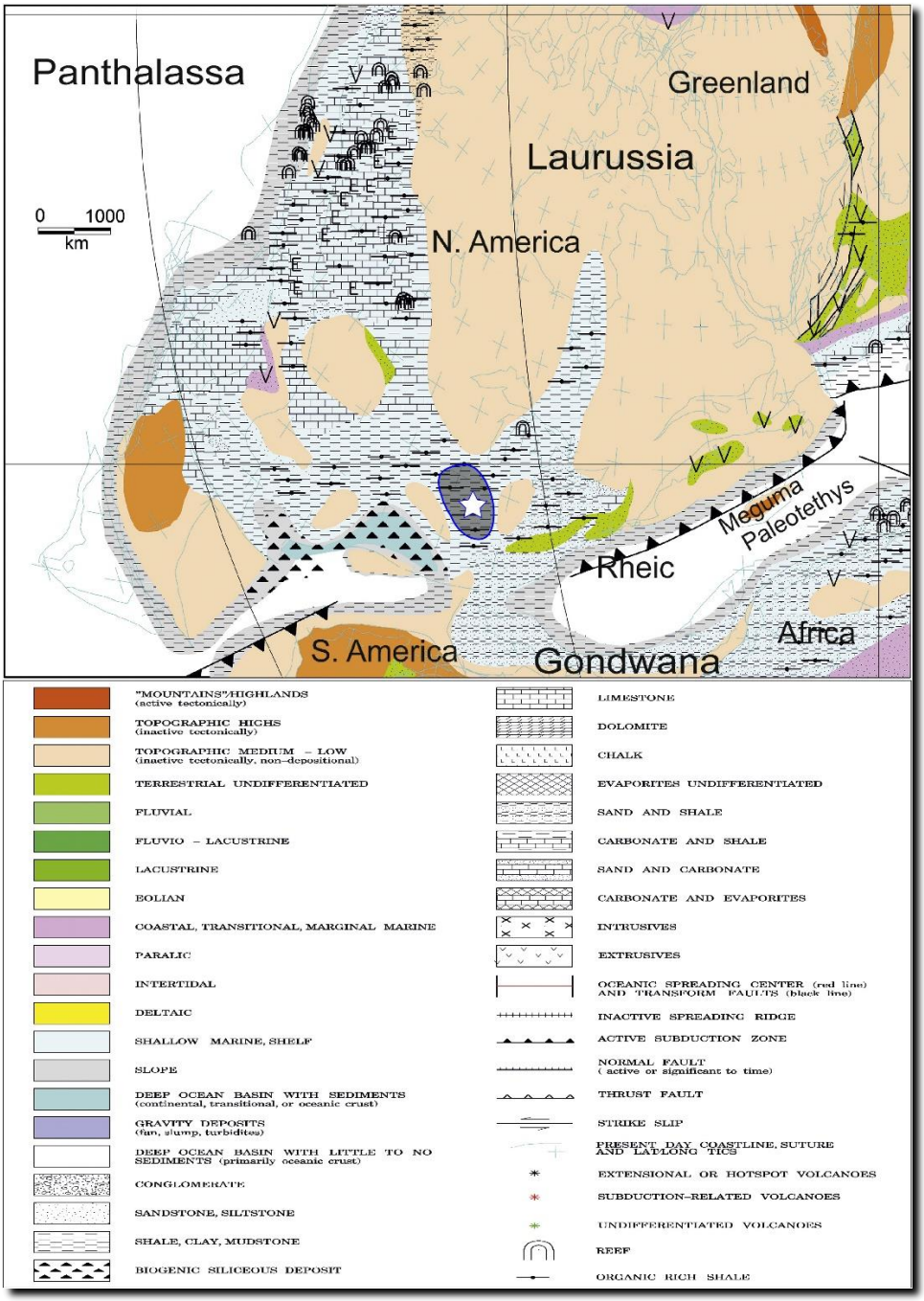

Fig. 3.4 *Local geologic setting of North America (i.e., Laurentia) during the Late Devonian, which was an integral part of Laurussia at this time. The white star indicates the position of the Illinois Basin. Modified from Golonka (2020)*

3.2 Devonian climate and oceanic anoxia

For most part of the Devonian, climate was generally very warm, and in large areas arid to semi-arid, only for it to start cooling down in the latest Devonian at the Frasnian to Famennian boundary interval (Zhang et al. 2021; Le Hir et al. 2011). A study by Zhang et al. (2021), proposed that in the Late Devonian and more precisely during the Frasnian to Famennian boundary interval, the planet experienced a transition from greenhouse conditions throughout the Frasnian into icehouse conditions in the Famennian. An $\delta^{18}O$ apatite oxygen isotope proxy (based on the analysis of conodonts) was used to prove an increased glaciation trend during the Famennian. It is suggested that when the levels of apatite in conodonts are low it means that seawater is diluted with $\delta^{16}O$, but if apatite levels are high, then it is proposed that temperatures have fallen and $\delta^{16}O$ is being precipitated at higher latitudes, thus causing glaciation. Another probable cause for the climate transition from hot to cold is the rapid evolution of terrestrial plants. CO_2 is a molecule that is released by volcanism, when levels of CO_2 surpass the ability of the ocean to absorb carbon, a heating effect is developed known as greenhouse effect. A reduction in CO_2 is seen during the Famennian, suggesting that the sudden sprout of plants may have been the reason for the cooling effect that took place in the Famennian. The common occurrence of carbonaceous material stored in sedimentary rocks of this age also support this notion (Le Hir et al. 2011). Golonka (2020), suggests that this change in climatic conditions could be due to hyper-volcanism found in places like the Siberian Traps (364.4 ± 1.7 to 376.7 ± 1.7 Ma.), or the many other active rifts and sea floor spreading ridges in the Devonian. During periods of extensive volcanism, large areas are prone to the influx of enormous amounts of ash, which also could lower temperatures enough to cause the formation of large polar ice caps and driving major sea level drops. Sedimentation in Laurussia during the Devonian was largely dominated by the deposition of continental red beds derived from the break-down and erosion of the Caledonian orogen and its many branches, resulting the accumulation of several kilometer thick succession of coarse-grained clastics in intramontane molasse basins. However, coal deposits in Arctic Canada and Svalbard (e.g., Janocha et al., 2024), also suggest some climate zonation superimposed on the otherwise prevailing and equable warm and dry climate.

Widespread anoxia has been recorded across the world through the Late Devonian. Places like central Europe, North America, and China have a few locations which can show signs of different causes, most of which are climate related, including fluvial drivers, sea level

change, vegetation, volcanic activity, or cooling. According to Bond et al. (2004), central Europe experienced anoxia due to sea level changes which caused upwelling of basal anoxic water onto the shallow epicontinental seas. Dunkel et al. (2022), states that modern day Baltic Sea experiences anoxic dead zones which are formed by the deposition of nutrients from rivers. Deltas are especially prone to having anoxic effect as they prograde. Based on that it is suggested that Appalachian Basin in North America may have been influenced by five transgressive – regressive cycles (Bond & Wignall, 2008) along with delta progradation with on occasional land organic matter input during intensive events like storms. An increase of Mercury (Hg) was recorded by Zheng et al. (2023), where it is believed that a Late Devonian vascular floral boom and increased nutrient input may have overloaded the water collum with Hg, which lead to the formation of Photic – Zone Euxinia (PZE). Volcanism has also been suggested as a leading driver, since an increase of CO_2 emissions have been recorded (Kabanov et al. 2023). Whether it is fluvial induced organic matter or nutrients, volcanic activity, or sea level change, all these examples are in some way tied to glacioeustatic regression. Copper (2002) suggests that in the Late Devonian the planet has transitioned from a greenhouse to an icehouse system by the occurrence of glacial events in the Famennian followed by intense highstand sediment propagation during interglacial periods. During that time the planet experienced the biggest O_2 enrichment versus CO_2 depletion. Volcanism may have been the first step during reconfiguration of cratons and the formation of volcanic arcs resulting in pumping the atmosphere with volatile gases like CO_2. Next, the formation of new mountain ranges in this case the Acadian and Caledonian orogens and subsequent erosion, gave opportunity due to the hot climate and increased humidity the formation of rivers, transporting sediment into basins like the Appalachian Basin (AB; see Fig. 3.5 for location). This hot climate in turn is favorable for vascular plants to take hold on land and expand dramatically causing Hg levels to increase within the water column while at the same time absorbing the previously released CO_2 and transforming it to O_2. The drop of CO_2 is the reason for icehouse effect to take place which in turn influences sea level behavior.

3.3 Structural framework of the Illinois Basin

The Illinois Basin in the Midwest of United States, is an interior cratonic type of basin, being 620 km by 375 km large. It hosts a seven km thick sedimentary succession of Cambrian to early Permian age (Dichiarante et al. 2021; McBride, 1998). The basin is defined by a series of structural elements, including the Kankakee Arch to the northeast, Cincinnati Arch to the

east, Nashville Dome to the south and Pascola Arch to the southwest (Fig. 3.5). Since the basin is located west of the Cincinnati Arch, it is too far away from the Acadian orogenic belt to be considered as a foreland basin. This designation is only valid for the nAB and sAB (Fig. 3.5).

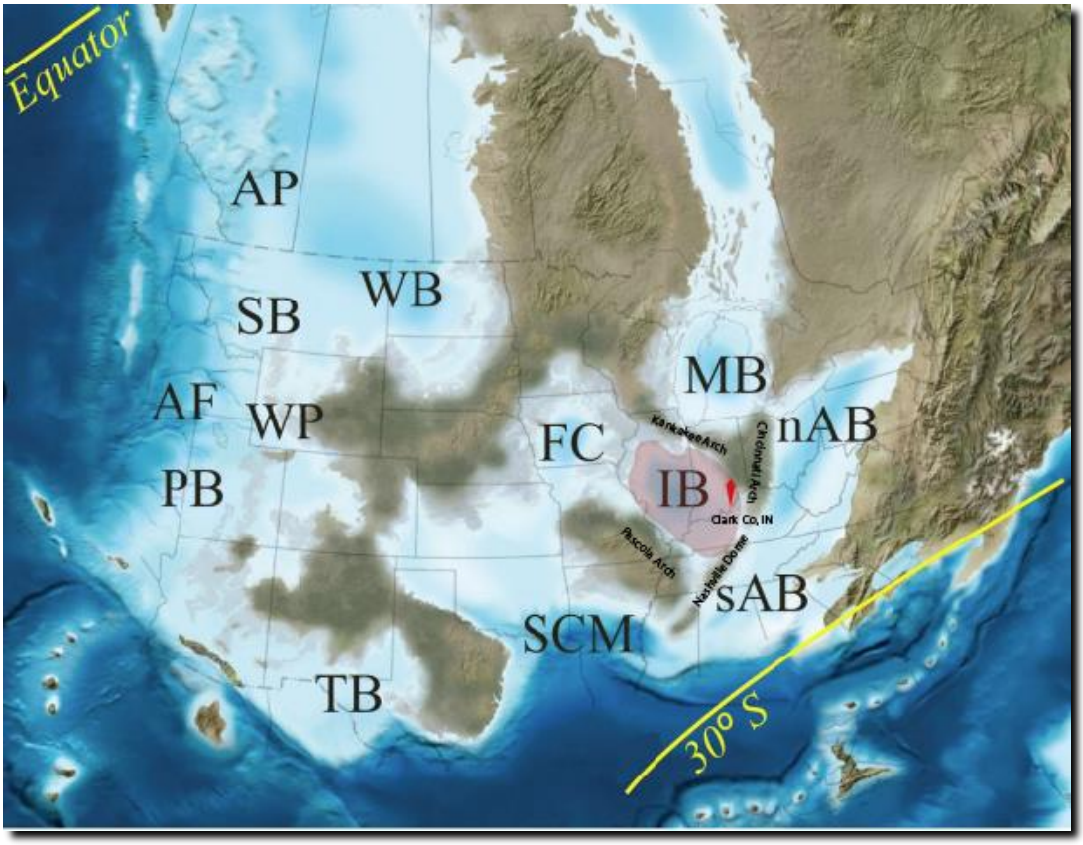

Fig. 3.5 *Late Devonian basins in Laurentia. Based on Over (2021). Base map from © Ron Blakey, NAU Geology. This thesis deals with the Illinois Basin (IB). Abbreviations: Northern Appalachian Basin (nAB), Southern Appalachian Basin (sAB); Antler Forland (AF); Alberta Platform (AP); Forest City Basin (FC); Illinois Basin (IB); Michigan Basin (MB); Pilot Basin (PB); Sappington Basin (SB); Southern Continental Margin (SCM); Tabosa Basin (TB); Williston Basin (WB); Western Platform (WP)*

Other important structural elements include the strike-slip and reverse faults, mainly located in southwestern side of the basin known as the New Madrid Seismic Zone (NMSZ) (McBride, 1998), La Salle anticline, Du Quoin monocline, and Cottage Grove fault system (Hatch & Affolter, 2002). A crystalline basement consisting of Proterozoic granites and rhyolites sits below the basin fill succession. The basin has experienced some volcanic activity as evident by intrusive breccia of late Mesoproterozoic age penetrating parts of the Paleozoic basin fill sequences (Freiburg et al. 2020) (Fig. 3.6).

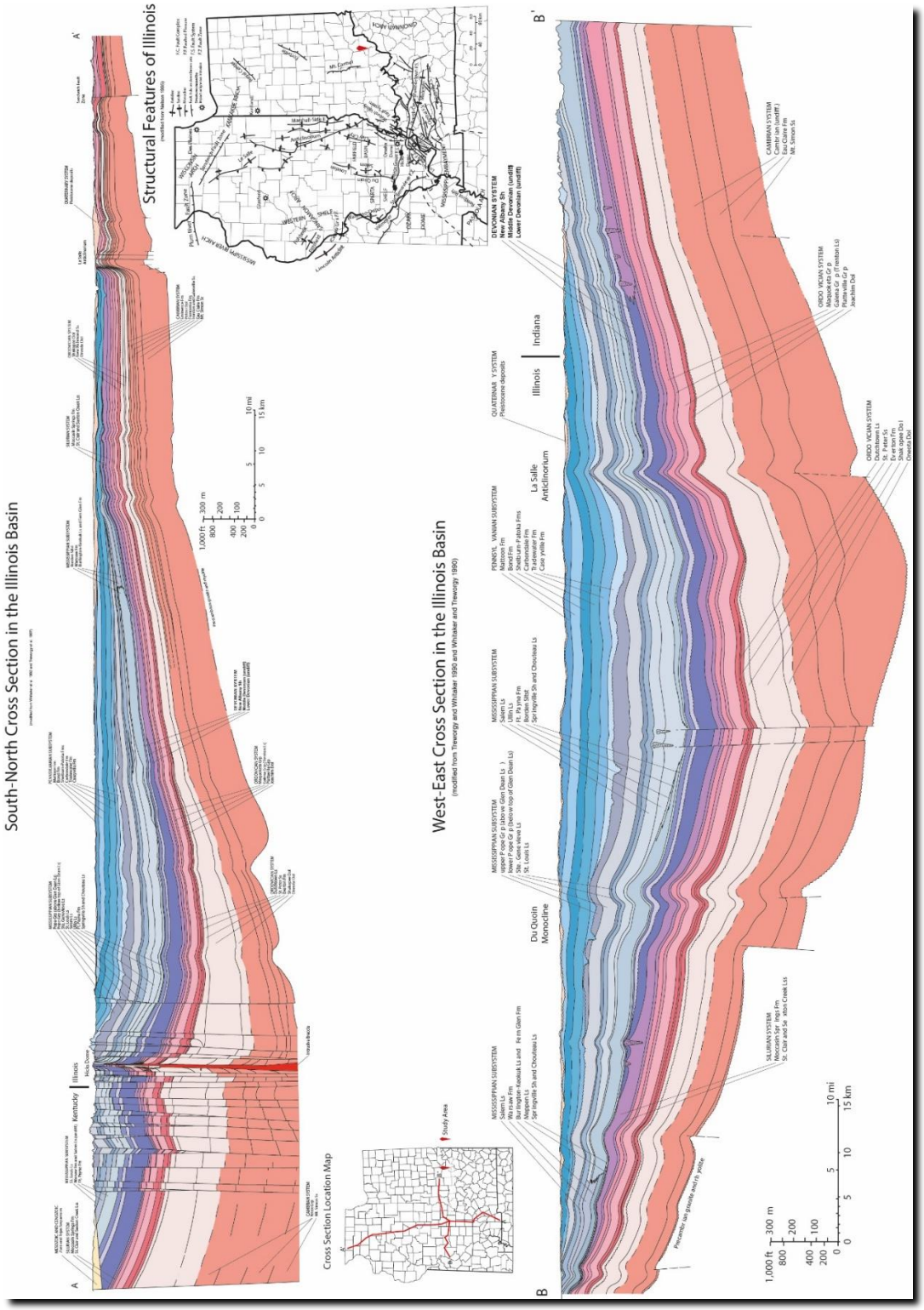

Fig. 3.6 *Illinois Basin cross sections showing stratigraphy, faults, magmatic structures. Edited from original: imap14-back.pdf (illinois.edu)*

Initially during the Middle Cambrian, the basin experienced significant rates of subsidence and was covered by an open-marine epicontinental sea until the Late Devonian, which collectively

allowed for near continuous sediment deposition during the early Paleozoic, accumulating an up to 6000 m thick sedimentary succession spanning the Cambrian to the Mississippian (early Carboniferous). In the late Paleozoic due to tectonic uplift and inversion of the basin margins, induced the development of the Pascola Arch to the south along with Cincinnati Arch to the east, the basin ultimately transformed into a landlocked depression which became a cite of significant mud deposition, also fostering anoxic conditions (Heidlauf et al. 1986). Uplift was caused by igneous intrusion, which in turn resulted in the erosion of overlaying sediment (Rabak et al. 2011). It has been suggested that the basin formed and evolved due to intracratonic subsidence caused by major rifting due to a mantle plume intrusion in the middle Cambrian (Heidlauf et al., 1986). Two separate driving mechanisms may have been responsible for the subsidence, the first being fault-generated subsidence, and the second being thermally controlled subsidence caused when the mantle plume cooled down and retracted. Post Devonian tectonic subsidence continued for an extended period between the middle Mississippian and early Permian (Heidlauf et al., 1986) resulting in even more sediment deposition leading up to yet another oceanic anoxic event and mass extinction at the end of the Permian-Triassic.

3.4 Lithostratigraphy of the Illinois Basin – the Devonian depositional system and the New Albany Shale

The two basin margins in the East and West, hosts entirely different stratigraphy. The East side is dominated by the Clegg Creek Member of the New Albany Shale, and the West is predominantly made up by the English River Formation, composed of gray shales and siltstone, possibly reflecting sediment influx from distinctively different source areas (Over, 2021). This study only pertains to the strata on the eastern basin margin, focusing on parts of the New Albany Shale.

According to previous investigations (Campbell, 1946; Lineback, 1970; Hasenmueller et. al., 1981), the New Albany Shale consists of five identifiable members in ascending order: the Blocher, the Selmier, the Morgan Trail, the Camp Run, and the Clegg Creek Members (Fig. 3.7), some being separated by regional unconformities. The Blocher Member is made of calcareous and non-calcareous brownish-black shale. Calcareous shale is concentrated at the base of the units, while dark limestone with pyritic laminations (Hasunmuller et. al., 1981), as well as sandstone (Campbell, 1946), are found at the top. This member has the greatest

concentration of organic matter, measuring up to 20%. The Selmier Member is composed of quarzitic sandstone beds with a mix of pyritic, dolomitic, and calcium carbonate laminations. The sandstone beds are commonly rich on organic matter. This member is not exposed in the study area of Clark County, Indiana. Besides pyritic laminae, euhedral pyrite, and pyrite filled spore exines have been reported (Lineback, 1970). The succeeding Morgan Trail, Camp Run, and Clegg Creek Members are uniformly similar, all containing fissile pyritic black shale with slight differences in color (Lineback, 1970; Hasunmueller et al., 1981). The New Albany Shale is approximately 30 m to 100 m thick, being thickest near the center of the basin, and time of deposition has been estimated to have occurred between 388–363 Ma (Heidlauf et al., 1986), thus spanning the Frasnian to Famennian boundary. This study focusses on the Camp Run Member, which is well exposed along road-cuts (of highway 311) in the study area in Indiana. Over time, the Illinois Basin has undergone various changes that are observable in the basin fill stratigraphy today. Through the Late Devonian, the Illinois Basin experienced four anoxic pulses, the first one being from the initial flooding of the basin, the second occurring in relation to a major regressive and progradational episode during the so-called Rhinestreet Event (biotic crisis), the third is linked to the Upper Kellwasser Event, which is attributed to sea level rise, and the last during a retrogradational phase which is marked by the maximum shale distal deposition across the basin (Ramirez et al., 2023). The mudstone deposits of the New Albany Shale are mostly laminated, bioturbated, or banded (thin siltstone/sandstone layers). Organic-rich, laminated black shales are commonly linked to anoxia which prevent bioturbation and promote organic matter preservation, and low energy, suspension settling in a quiescent environment below storm wave base Lazar & Schieber, 2004). Intensive erosional periods marked by distinctive layer differences with sharp contacts within the New Albany Shale suggest that the basin has been affected by periodic sea level changes or turbulent weather which have a lateral erosional effect on sediments. (Lazar & Schieber, 2022).

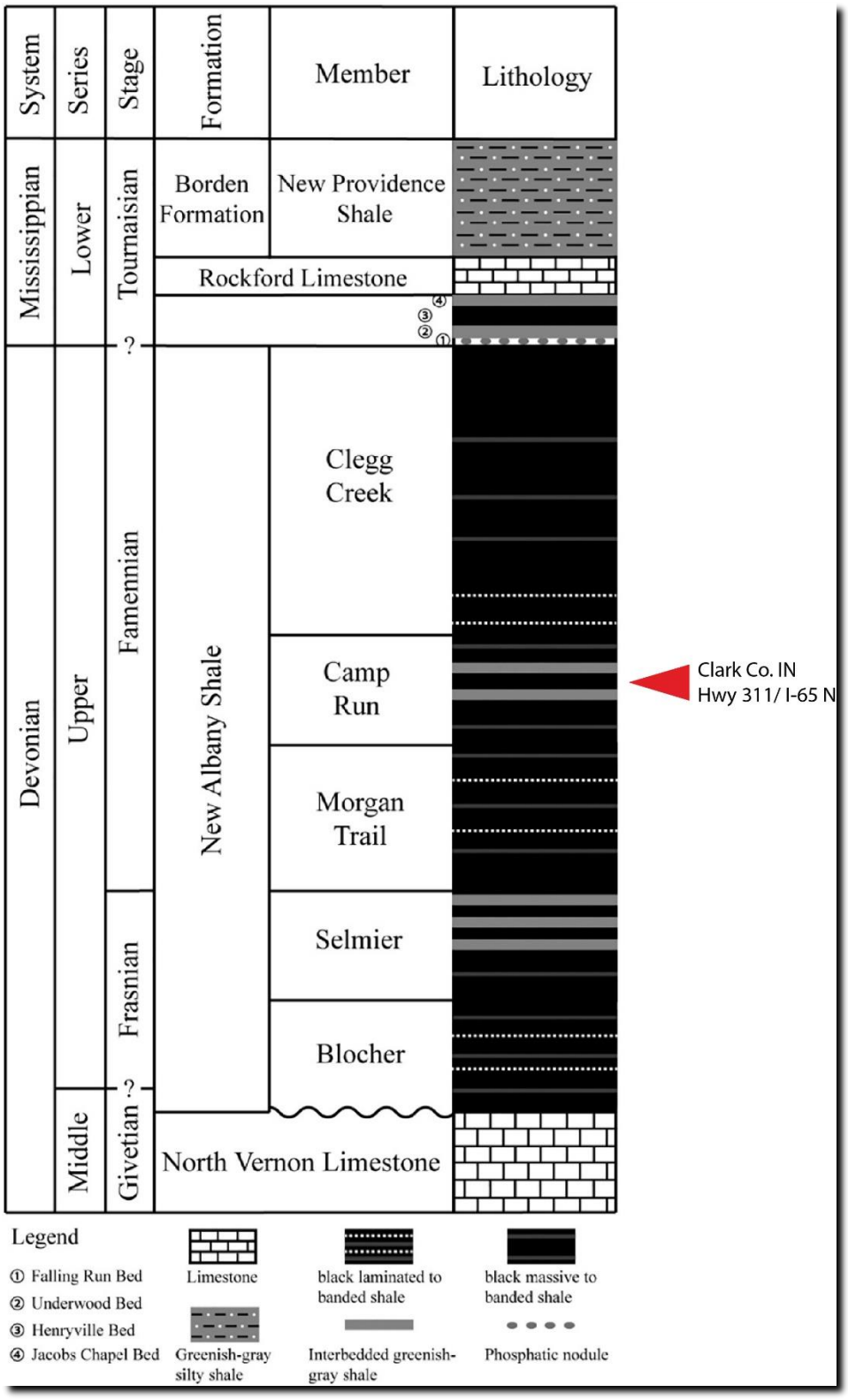

Fig. 3.7 *Stratigraphic column of New Albany Shale. The red triangle indicates the investigated unit (the Camp Run Member) and sampled interval. Modified from Liu et al. (2020)*

3.5 Oxygen conditions and metal enrichment during deposition of the New Albany Shale

It has previously been suggested that deposition of black shales in the Illinois Basin was caused by the landlocked nature of the basin due to the surrounding and uplifted arches (e.g. Lineback, 1979). These natural barriers restricted the basin from being affected by ocean currents that could oxygenate its waters and which could disrupt the accumulation of fine sediment. Moreover, landlocked basins with a certain influx of riverine water tend to develop salinity stratified water columns, with an upper freshwater layer promoting restricted and anoxic bottom water conditions (such as the present-day Baltic Sea) (Dunkel et al. 2022). The depth at which the investigated black shale was deposited is thought to have taken place at the shallow water depths, down to about a depth of 60 m, based on the findings of brachiopods in the shale (Lineback, 1970). The abundance of fine laminations in the shale succession suggests calm and quiescent waters below storm wave base, and the concurrent lack of coarse-grained sediment exhibiting traction generated structures support the notion of basin little influenced by currents. The general lack of fossils in the Devonian black shales of the Illinois Basin further indicate quite a volatile environment at the time of deposition. Some fossils do, however, occur in interbedded limestones beds (Collinson et al., 1967), and together with horizons of burrows in the shales (Wilson et al., 2021), this points to periods of oxygenated waters superimposed on the otherwise oxygen-depleted nature of the basinal waters. A general pre-conceived interpretation/conception for shales are that dark brownish to black shale indicates lack of oxygen and widespread anoxia during deposition, severely limiting the chances for life to thrive in waters and bottom sediments, whereas greenish to gray shale record deposition during moderate to well oxygenated conditions, typically giving room for some species to thrive in the water column and in the upper sediments. During anoxia, sulfate reducing bacteria begins to thrive and process organic matter into sulfides. Pyrite (FeS2) or iron monosulfide (FeS) (Wilkin & Barnes, 1997) appear within sediment beds, or in the cases of euxinic conditions, pyrite framboids may form in the water column to be deposited on the sea floor eventually becoming part of the finely laminated sediment hosting them. Pyrite framboids can be formed in non-anoxic conditions but hydrothermal solutions of up to 200^{o} C must be available (Wilkin & Barnes, 1997), in the case of the Illinois Basin, no such conditions have persisted, leaving anoxia as the only option. Pyrite has been widely reported in the organic-rich black shales of

the New Albany Shale, all pointing to anoxic conditions during deposition. According to Lineback (1970), organic matter is found uniformly distributed in the shale across the basin, possibly owing to the algal blooms as indicated by the presence of algae like *Tasmanites*, *Foerstia* and *Protosalrinia*. Such algal blooms are known to consume the oxygen of the surface waters causing anoxia in the basin. Soeder (2018), further suggests that seasonal algal blooms could cause this uniformity of organic carbon to be present across the shale basins. As these episodic blooms continued over time, whether they were seasonal or induced by volcanism (Lin et al., 2023), organic matter was preserved and eventually turned into hydrocarbons. Intriguingly, Wilson et al. (2021), recently suggested that pyrite in the Devonian strata of the Illinois Basin formed under non-anoxic conditions despite being present in black shale deposits. Not all members of the New Albany Shale were deposited under the same conditions, the Clegg Creek Member for example, has been affected by anoxic to euxinic conditions (no oxygen with presence of sulfur), while the Camp run has experienced anoxia and occasional low levels of oxygen (dysoxia). The least affected units by anoxic conditions were the Morgan Trail and Blocher Members (Ocubalidet, 2013). This variations on oxygenation may affect the abundance of pyrite within members. According to (Koslowski et al., 2016), pyrite crystals which are only detectable with the use of a microscope can be explained only by the presence of sulfate reducing bacteria as these crystals are too small to be formed diagenetically. The carbonate content of the shale succession varies and is mainly derived from sulfate reducing bacteria forming calcite or dolomite, which are found in abundance in the Blocher and Selmier Members (Lineback, 1970). Another biochemical product seen is hydro troilite ($FeS.nH_2O$), over time it breaks down to pyrite and marcasite (Lineback, 1970).

Various metals have been reported in the New Albany Shale (Ripley & Shaffer, 2000). Since the study location is at the very margin of the basin near the eastern extent of the New Albany Shale group and close to the Cincinnati Arch, it can be assumed that the investigated strata were deposited relatively near the paleo-shoreline. This proximity to land, also opens for significant contributions from terrestrial organic matter (OM) than marine. These two sources of organic matter flux have different exposure to metals absorbed from the ground. Therefore, marine OM will be concentrated with certain trace metals, while terrestrial OM would be the source of other metals (Algeo et al., 2007). Coastal environments are subject to mixing of sediments from land and sea. Fluvial systems bring OM from surface runoff enriched in metals like Barium (Ba), Manganese (Mn) and Tungsten (W), while marine OM is mostly enriched in

Molybdenum (Mo) derived from phytoplankton blooms (Speidel et al., 2024). The location in Sellersburg, Indiana exhibits many metals that could have been derived from various sources. Trace metal concentrations are dependent on factors such as sedimentation rate, water column reduction conditions, rate of organic matter supplied and trace metals brought from within deep ocean (Abdi et al., 2024). The importance of studying trace metals is that we can learn about the intensity of biological recycling in oceans as these metals are the byproducts of such processes (Brumsack, 2006). Traces such as Cadmium (Cd), Cobalt (Co), Copper (Cu), Nickel (Ni), Lead (Pb), Selenium (Se) and Zinc (Zn) are some of the more common elements found within framboidal pyrite in the New Albany Shale (Tuttle et al., 2009).

4 Methodology

Samples for this project come from a small outcrop of Late Devonian-aged black shale occurring adjacent to Highway 311 (Charlestown Rd) in Sellersburg, Indiana, USA. Coordinates of the location are 38°23'33"N 85°45'49"W, with the sampled section spanning from 146 m above sea level at the base to 151 m above sea level at the top. The section (Fig. 4.1) was briefly described and documented to provide a stratigraphic framework for the collected samples. The outcrop was chosen because of its nice exposure being one of very few places where shale is not entirely covered and buried by younger rocks, which typically is the case in more central parts of the Illinois Basin.

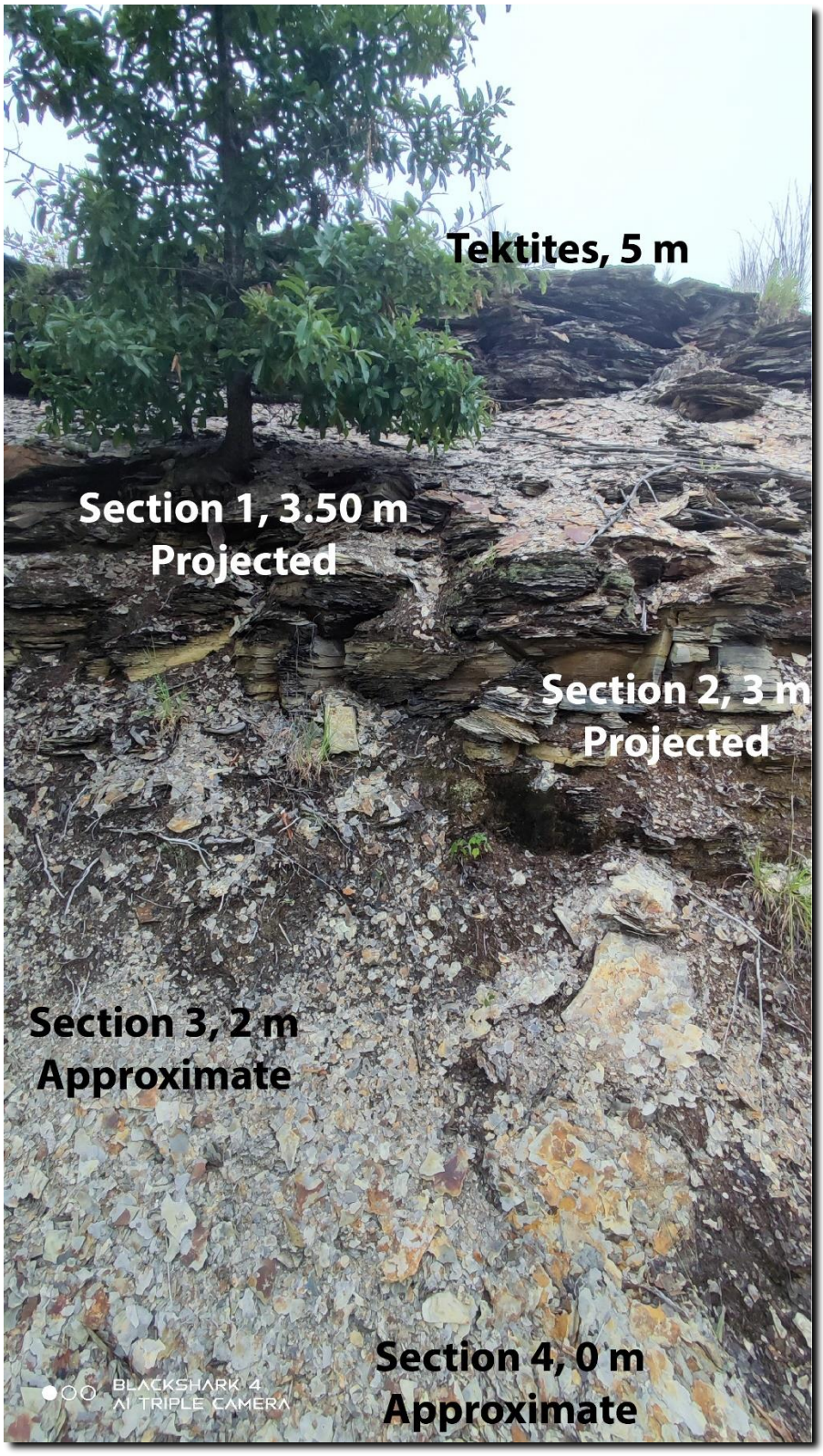

Fig. 4.1 *Photograph showing general location of rock thin sections and lose material collected for tektite analysis.*

Collection and preparation

A total of one bulk sample was collected for multiple geochemical and petrographical analyses. The collected material was taken to (Indiana University Southeast geological lab) where it was dispersed on a pan to properly dry since shale tends to keep moisture between its delicate layers. Once dry, the shale was sieved to separate unwanted particles. No additional treatment was needed. The process required the use of five different sieve sizes, starting with 1.18 µm, 600 µm, 300 µm, 100 µm, 75 µm and lastly all smaller particles were captured by the bottom pan. Sediment from the smallest size was used to prepare carbon stubs with microtektites meant to be analyzed under SEM with the use of magnet for their extraction. The particles believed to be tektites are highly magnetic which makes them very easy to sort out from the rest of the sediment. During the preparation of the stubs not one pyrite grain was picked up by either a magnet or a picking tool because the mineral is essentially nonmagnetic.

Since shale tends to break into flakes, finding a well-preserved thick piece for thin-section production is a challenge. However, four hand-sized slabs were collected from different parts of the investigated interval with the aim for them to be prepared into thin sections and further petrographic analyses.

Raman microscopy

An attempt was made using Renishaw inVia Raman microscopy to investigate certain structures within thin sections. This instrument works on the principle of using a laser which is focused on the point of interest. The targeted location's molecules begin to vibrate, and radiation emitted will either be scattered, absorbed, or reflected, giving a graph of a specific mineral signature.

X-ray fluorescence (XRF) and X-ray diffraction (XRD) analyses

One shale sample was sent to the Earth Surface Sediment Laboratory (EARTHLAB) at the University of Bergen (UiB), for XRD and XRF analysis. An ITRAX X-Ray Fluorescence (XRF) instrument was used to scan the sample. This instrument is used to find the elemental composition of a rock or sediment. The sample is being exposed to high energy radiation which causes atoms within sediment to start releasing electrons from the center, and when electrons from the outer layers migrate to the middle, fluorescent radiation is produced which is being

translated into data. According to EARTHLAB, most of the produced data is semi-quantitative because of the possibility of inconsistencies caused by factors such as grain size, water content, and other factors. A Bruker D8 Advance Eco X-Ray Diffraction was used to determine the mineral composition of the sample. This process maps out mineral structure, by diffracting x-rays through its crystal forms. This method is used to give more of qualitative analysis of overall sample.

Conventional microscopy

Unravelling the origin and nature of microtektites, and to separate these from other spherules, requires the study of their chemical composition and surface topography (at micro scale). Thus, the use of different types of microscopes is necessary to analyze, in detail, what they are made of and how they appear up-close. The four thin sections were examined under a conventional petrographic microscope allowing for investigations under plane and cross polarized light. Plane/reflected light is useful to distinguish pyrite because it reflects light and has a bright yellow appearance, while tektites are not visible at all. Cross polarized light shows both grains, leading to a difficulty figuring out which grain is what, since tektites depending on makeup have opaque (contain an oxide) or isotropic (contain Si) properties. The distinguishment between microtektites and pyrite can thus be a challenge because pyrite may occur as tiny framboidal aggregates which resemble spheres. Thin sections were investigated using Leica DM 4500 P with LAS X (Leica Application Suite X) imaging software. In the process, images were taken showing pyritic framboids along with tektites. Additionally, Leica Z16 APO microscope was used to take photographs of individual tektites in 3 dimensions.

Scanning electron microscopy (SEM) and energy dispersive X-ray spectroscopy (EDS)

The most time-consuming method applied in this study, is the use of the TM3030 Tabletop SEM – Bruker Quantax 70 EDS instrument, which works on the principle of shooting electrons at grains, which in return glow allowing for an image to be produced. All of this happens in a completely dark and vacuumed chamber. SEM is the image processing unit which allows magnification up to 30 000 times for high resolution photos of micro-topography and other micro-scale features that can be identified on the surface of the investigated grains. EDS is the component required for the chemical composition analysis to be completed. It works by

reading X-ray energies released by elements found in each specimen when they are struck by electrons shot from the detector. Each element on the periodic table corresponds to an X-ray peak signature, as the process runs, a graph is produced displaying multiple peaks of the most dominant elements of the targeted grain.

5 Results

5.1 Raman Microscopy

Raman was used to analyze a few structures that could represent the previously mentioned Lonsdaleite (type of diamond formed by shock metamorphism). Unfortunately, this speculation was proven wrong as the laser used in the analysis, even at the lowest setting, was burning through the thin section and no substantial findings were discovered. Pyrite was also subject to Raman microcopy analysis for a quality check and to confirm that it was pyrite (which most definitely was), but no results were gathered and saved due to its well-known existence within the shale beds (as also shown by the other methods).

5.2 Bulk X-ray fluorescence (XRF) and X-ray diffraction (XRD) Analysis

XRF analysis was done, although, due to the magnetic nature of the tektites and their sizes, picking even a few cubic centimeters (i.e. the minimum volume required for analysis) of such particles is very time consuming. Instead, bulk sediment was tested rather than specific particles. Overall, 34 elements were identified in the analyzed bulk sample, of which 5 (indicated in bold names) have previously been considered as trace metals specific for the New Albany Shale within the Clegg Creek and Camp Run Members (Beier & Hayes, 1989). Trace elements identified are as follows: Aluminum (Al), Argon (Ar), Barium (Ba), Bromine (Br), Cadmium (Cd), Calcium (Ca), Cerium (Ce), Chlorine (Cl), **Chromium (Cr)**, **Copper (Cu)**, Gallium (Ga), Gold (Au), Iron (Fe), Lanthanum (La), Lead (Pb), Manganese (Mn), Mercury (Hg), Molybdenum (Mo), **Nickel (Ni)**, Phosphorus (P), Platinum (Pl), Potassium (K), Rubidium (Rb), Selenium (Se), Silicon (Si), Strontium (Sr), Sulfur (S), Tantalum (Ta), Tin (Sn), Titanium (Ti), Tungsten (W), **Vanadium (V)**, Yttrium (Y), **Zinc (Zn)** and Zircon (Zr). Of those listed, Y, La, Ce are considered Rare Earth Elements (REE). The possible explanation behind their appearance could be due to very small traces or scattering anomalies. Since the XRF analysis was done to a single batch, only qualitative results are obtained pertaining to the

general composition of the sediment, if a more precise quantitative data was needed another complementary sample would have had to be tested.

In contrast to XRF, the XRD doesn't need a base to achieve a quantitative result. This method shows an overall dominant composition of the whole sediment sample instead of looking for specific trace elements. It is thus concluded that the analyzed sample predominantly consists of quartz (SiO2), which is not a big surprise given the siliciclastic nature of the shale. The overall content from the XRD analysis is shown in the graph below (Fig. 5.1)

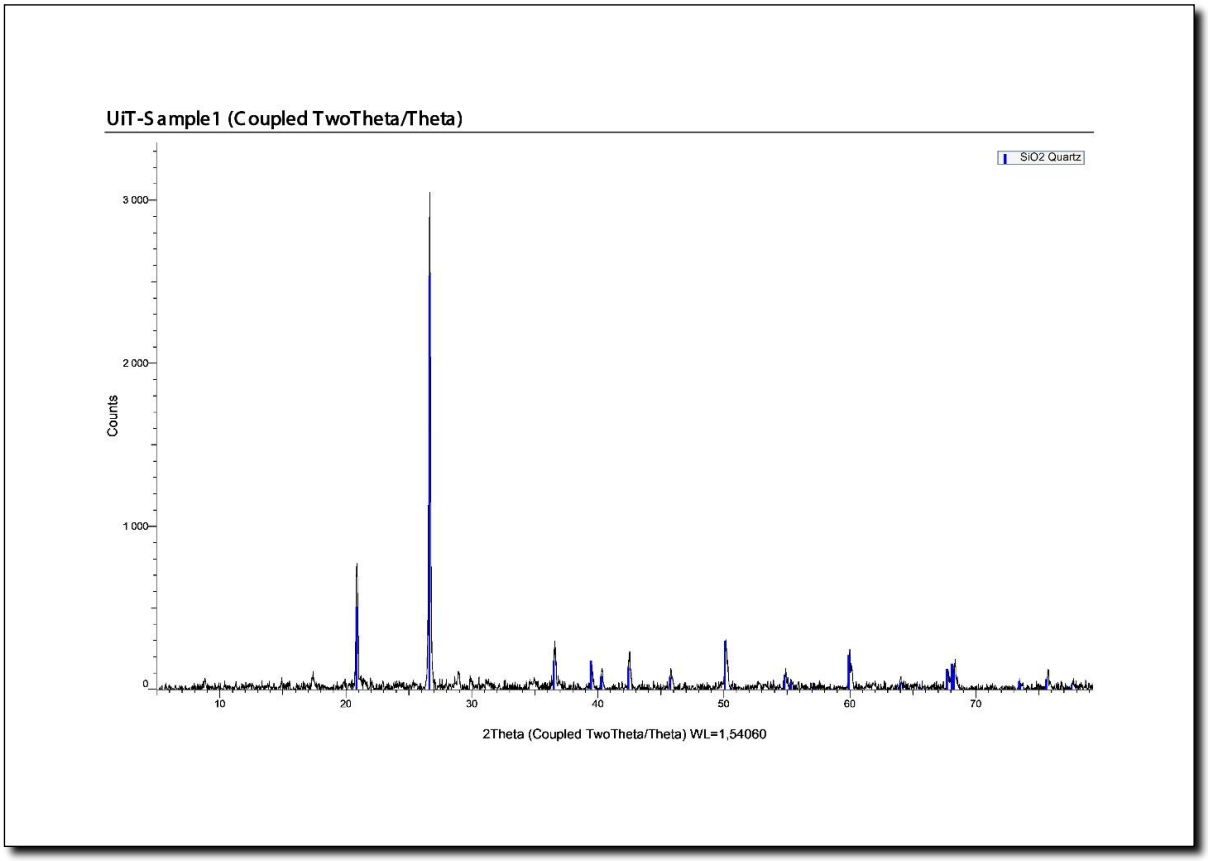

Fig. 5.1. *Silica peaks acquired by XRD analysis showing the general quartz-dominated composition of the shale.*

5.3 Conventional microscopy

Four thin sections were prepared and sequentially observed under petrographic microscope (Section 1, Section 2, Section 3, Section 4). Three of the thin sections represent an OM rich and finely laminated portion of the Camp Run Member (Fig. 5.2 B) (Fig. 3.7 for stratigraphic position; thin sections 2, 3 and 4). The last thin section (1) varies dramatically, since it's mostly composed of a well-cemented (quartz) and more massive appearing mudstone

containing lots of pyrite (Fig. 5.2 A). Along with the pyrite, microtektites are also observed in Section 1. Although the thin sections show an abundance of pyrite, that is not the case with the particles observed on carbon stubs. Most of those particles are highly magnetic making them easy to pick up with metallic tools allowing for their relocation onto the carbon tape. Structures like framboidal pyrites, microtektites and *Tasmanite* algae have been recorded, and lastly a potential shocked quartz. Below follows detailed descriptions and interpretations of the various particles recognized in the thin sections, focusing particularly on the pyrite, microtektite, and *Tasmanites* particles, which all are of great importance with respect to the following discussion chapter. Quartz grains, which are the most common constituent of the shales, organic matter, and subordinate mica grains of various composition, are only treated superficially here (only marked on some thin section photographs) as they are very common type of grains/particles described and dealt with in numerous other thin section studies elsewhere (e.g. Bolton et al., 2004; Lineback, 1970; Wilson et al. 2021).

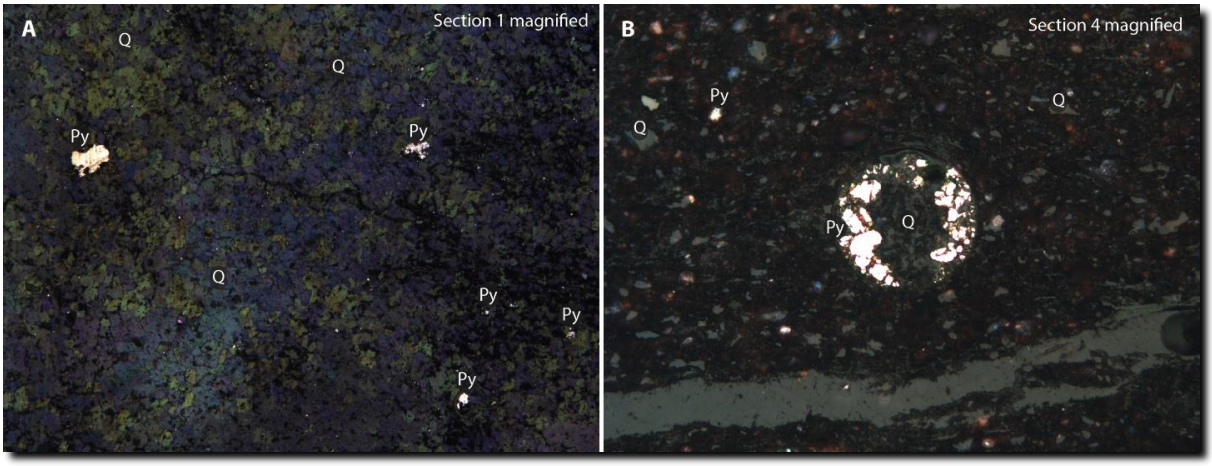

Fig 5.2 *A) shows composition of Section 1 being dominated by quartz and pyrite. B) represents the rest three sections since all of them are similar in depositional features and content.*

Pyrite framboids

Description

Framboids, comprising multiple spherical grains, like the one seen in Fig. 5.3, occur in clusters no more than few of tens of microns in size. The image bellow is a formation observed under reflected light giving it a yellowish hue.

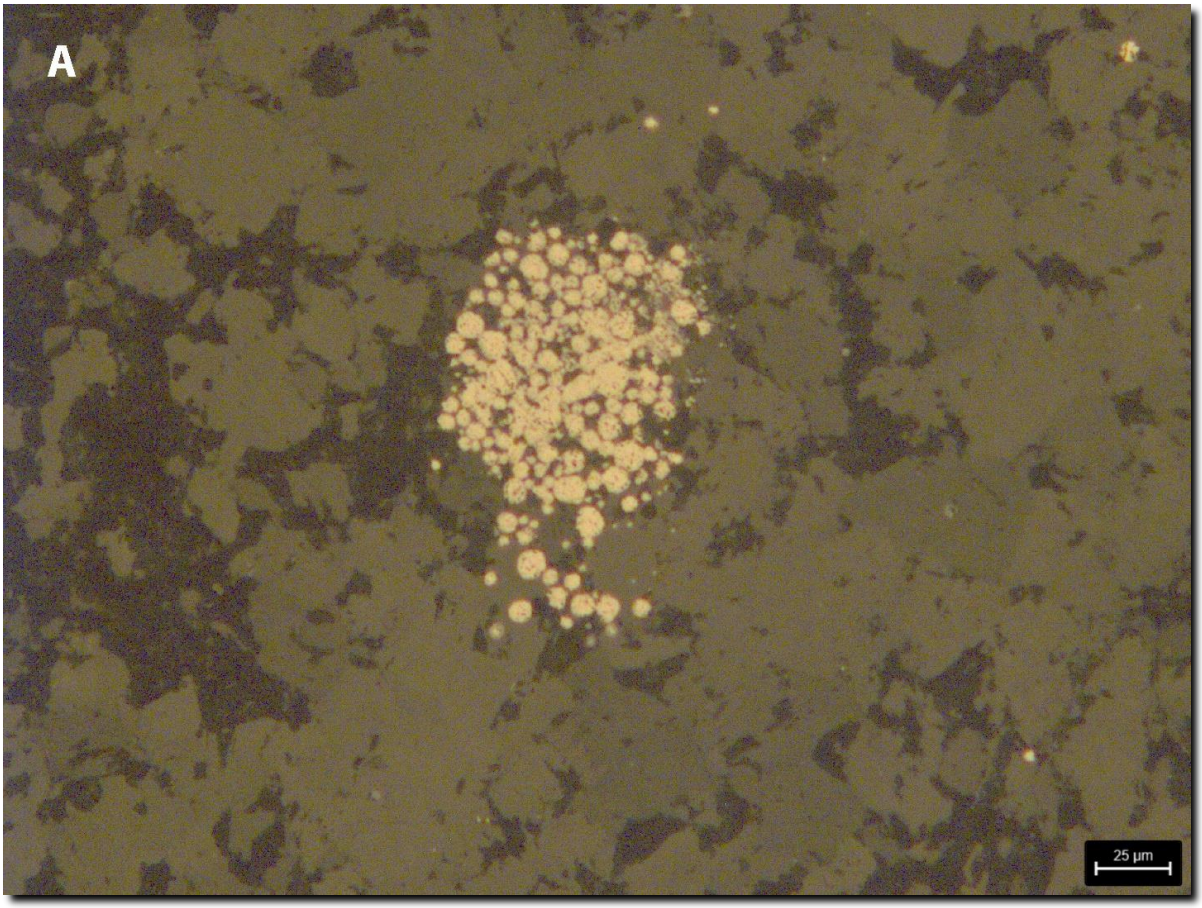

Fig. 5.3 *Example of framboidal pyrite (thin section 1). They typically start as clusters like these which resemble spheres and may later transforms into the well-known cubic form after multiple recrystallization phases (Zhao et al., 2018).*

Interpretation

Pyrite forms in two distinctive ways, 1) framboids influenced by organically rich sediments, and 2) euhedral (cubic) formed from solution (Sawlowicz, 1993). Wilkin & Barnes (1997), suggest that framboidal pyrite forms in a four-step process: iron monosulfide crystal formation

occurs first, then crystals interact with greigite, aggregation begins of greigite and eventually it is substituted and taken over by pyrite adopting the framboidal form. Pyrite is merely a byproduct from the aggregation of magnetic framboids like greigite or magnetite (Wilkin & Barnes, 1997), these sulfides may be highly magnetic, but once pyrite begin forming it is considered as nonmagnetic since the leftovers of the previous material have very weak magnetism within its structure. As suggested by Bolton et al. (2004), pyrite formation becomes scarcer as the stratigraphy transitions from inorganic sediments to organic rich sediments. This occurrence can be observed here, where most of the well-developed pyrites are in thin section 1, which is quartz dominated and not much of organic matter is available.

Pyrite - microtektite co-occurring assemblages

Description

Both pyrite lumps and microtektites, no more than 20 µm across, may co-occur and form closely related grain assemblages (Fig. 5.4). The quartz dominated thin section (1) has the most abundant concentration of these co-occuring spherule assemblages. While pyrite doesn't allow for light to go through it, depending on composition, some tektites clearly appear to react to polarized light. Tektites thus come in many colors. Every pyritic framboid is solid from the start and maintains its honeycomb appearance until it transforms into a more polygonal cubic look.

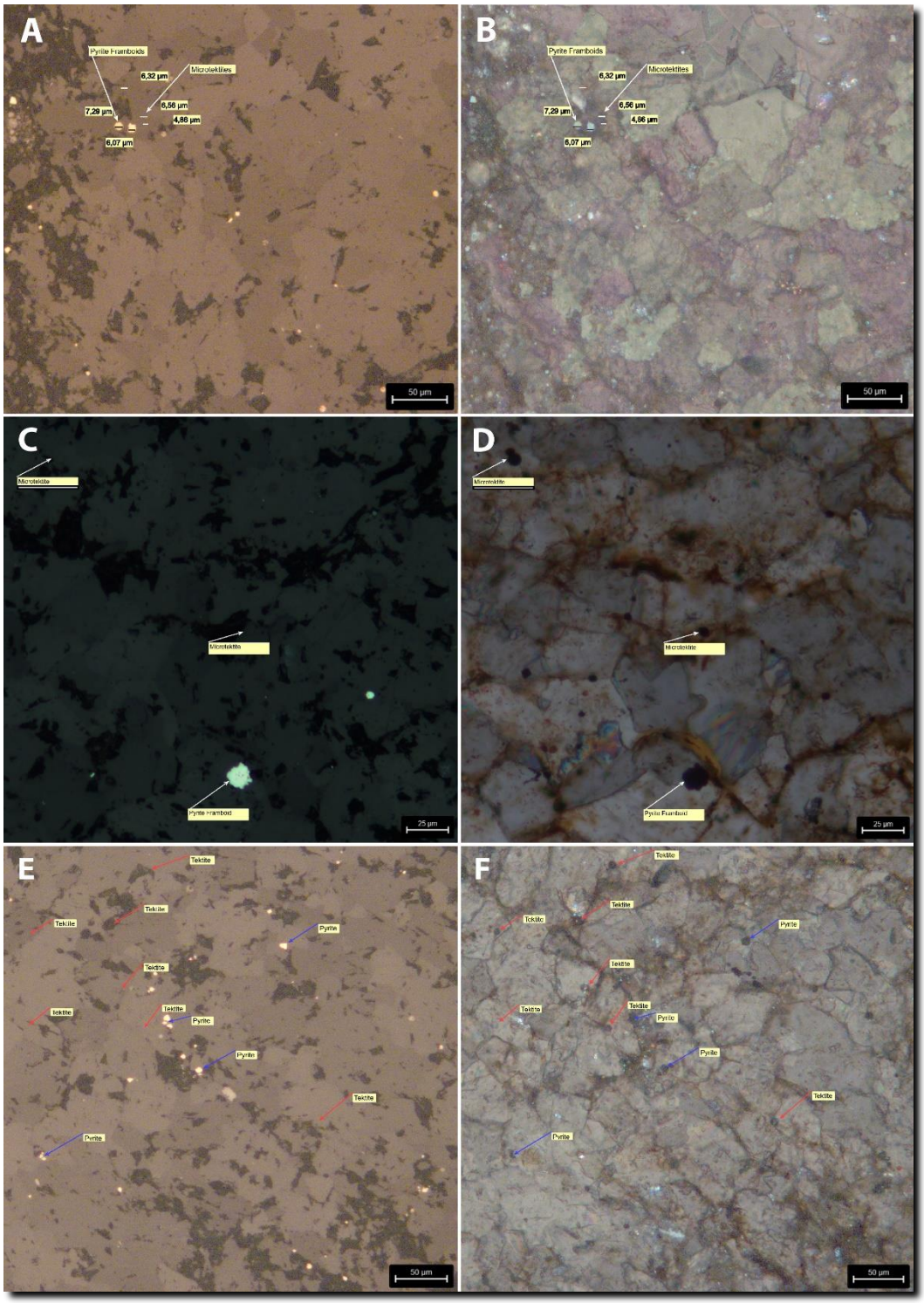

Fig. 5.4 *Combinations of co-occurring assemblages of microtektites and framboidal pyrites. Three separate sets of assemblages within thin section 1. Photographs: A, C and E show pyrite glowing with a yellow hue under reflected light. Photographs: B, D and F show cross polarized images where pyrite framboids and microtektites can easily be mistaken for the other. Image F shows a distinctive shimmer to the microtektites, which is not found on pyrites.*

Interpretation

Comparing the pyrite grains and roundness of tektites, it can be assumed that pyrite may have begun forming post tektite deposition. Every instance of microtektite cluster is near pyrite but not every pyrite cluster has microtektite groups nearby. Since most of the mafic microtektites are composed of metals like magnetite (Kleinmann, 1969) and formation of pyrite requires the aggregation of greigite or magnetite (Wilkin & Barnes, 1997), it can be assumed that in the case of Fig. 5.4, tektites may have been deposited first and seeding the sediment with metals giving possibility for pyritization to occur over time. Another clue that microtektites are first is that majority of pyrite, although being spherical, they commonly tend to exhibit angular shapes suggesting later in time genesis.

Single/solitary tektites

Description

Below Fig. 5.5 shows examples of single tektites found in the OM rich thin sections (thin sections 2, 3, and 4). These slides have 50/50 ratio of OM and quartz. Matrix color may be due to oxidation of iron giving it the red coloration. Pyrite is present, but not in the similar abundance like in previous figures (from thin section 1; Fig. 5.4), but as single and isolated grains (and never in clusters). Same goes for the microtektites as three separate instances of single spherules are shown below. As seen in the reflected light images, the spherules are hollow in nature.

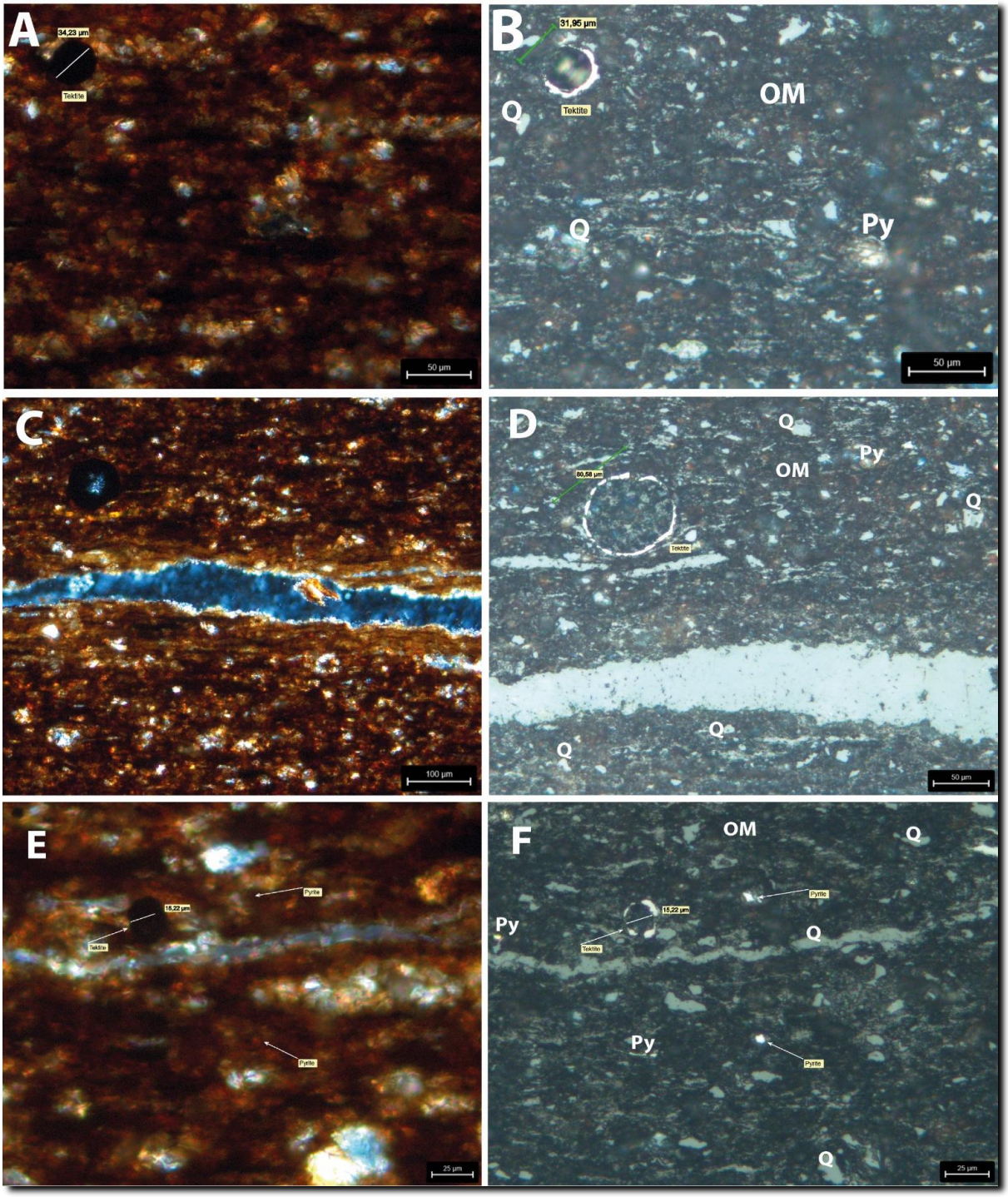

Fig. 5.5 *Microtektites showing internal structure.*

Interpretation

Given the isolated occurrence and general scarcity of tektites close to pyrite grains, it appears as these two grain types seem to coexist in quartz dominated facies and very limited

assemblages are occurring in the OM rich sections. Similarly, Bolton et al. (2004), suggest that pyrite tends to not be present in OM rich layers as it oxidizes faster and possibly giving the reddish hue of the laminae. Oddly enough, compared to previous reflected light images here tektites do show up. This can be a result of their metallic composition while others are more silica based. Images B, D, F in Fig. 5.5, give a glimpse of what the internal structure looks like for a hollow spherule. Microtektites come both in solid grains and some may even be hollow due to expanding gasses (Suttle & Genge, 2017) during reentry, therefore these grains can be mistaken for pyrite, if they happen to be solid and observed in a thin section. Tektites are systematically described and categorized later in this chapter based on the SEM analysis.

Tasmanites

Description

Oval to circular grains with sizes ranging between 200 to 350 µm, occurring in multitude of colors, but most commonly exhibiting a reddish hue are found in thin sections 2, 3 and 4. Not one was found in section 1. Image (A) and (C) in Fig. 5.6, shows what in general Tasmanites look in loose sediment, where two different appearances are seen. Some are more deformed while others retain their original shape.

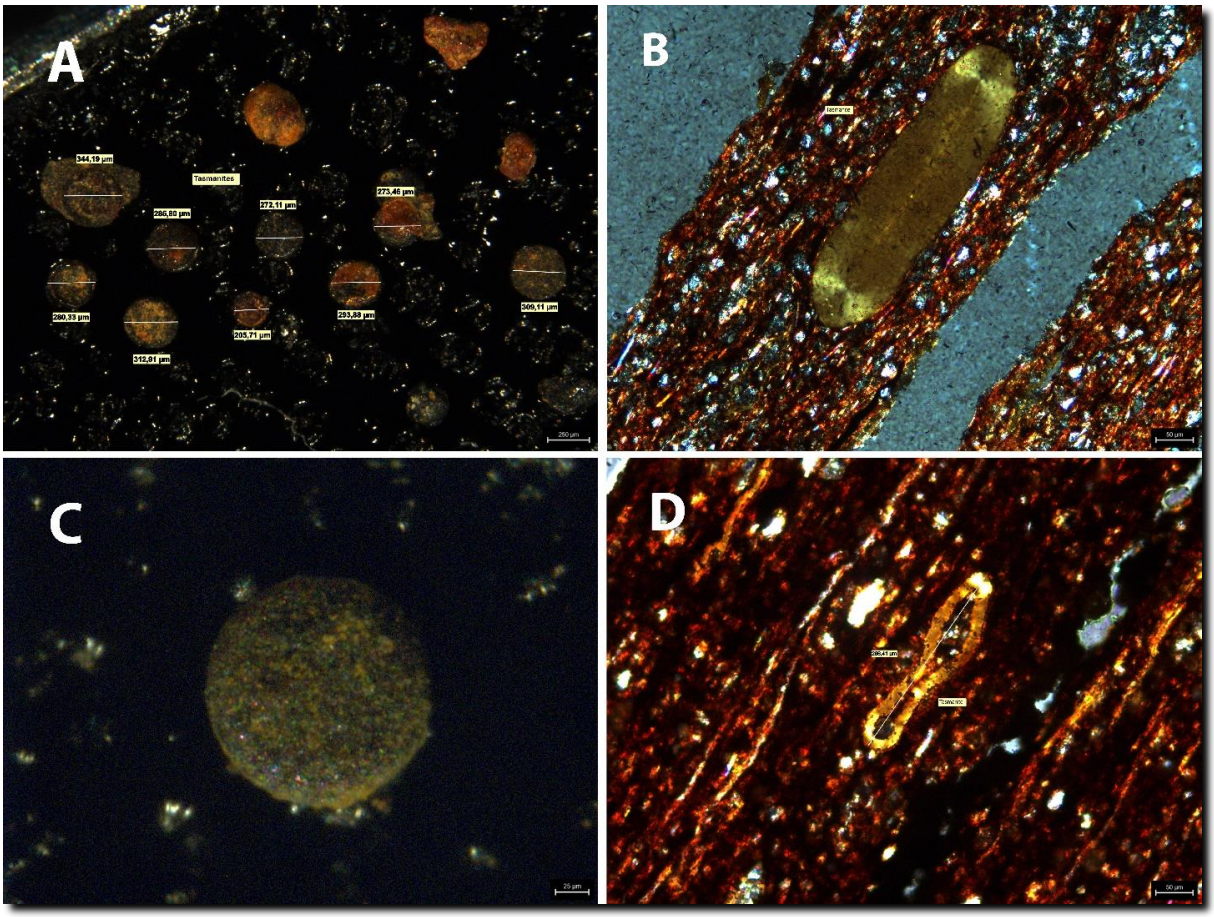

Fig. 5.6 *3-dimensional (A and C) versus 2-dimensional (B and D) view of tasmanite algae.*

Interpretation

Arthur & Sageman (1994), suggest that sediment rich on OM derived from algae is considered as "sapropel", which is term defining a black shale that has been deposited in oxygen depleted interval during water stagnation. This means that only laminations containing algal matter such as Tasmanites can be seen as sapropel like in thin section 2, 3 and 4. Based on the shape and color, the reddish-colored (oxidation or mineral substitution) grains are interpreted to be *Tasmanites* algae. These algae live in the water column absorbing CO_2 and releasing O_2. When these microscopic organisms die, they sink to the bottom where bacteria decompose them, and oxygen gets depleted in the process. This process leads to the establishment of oxygen minimum zones (OMZs). They are likely to develop on the margins of basins, just like the studied location (Arthur & Sageman, 1994). By having many traces of this microorganism, means that at some point anoxic conditions were present at the location. Algal blooms can decrease CO_2 levels and potentially lower atmospheric temperature, but at the same time when

the blooms die, anoxia is initiated due to overload of organic matter that sinks to the bottom (Pippenger et al., 2023). There is a visual difference between tasmanites shown in Fig. 5.6 (B) and (D) and the matrix surrounding them. It can be assumed that (B), has been more tightly compacted thus causing for the algae to have no sediment in the middle, while *Tasmanites* on (D), may have absorbed some sediments before it got deposited or may have gotten filled in post deposition during burial.

Potential shocked quartz grains

Description

Images bellow show some potential shock metamorphism. Distinctive features of such grains are light refraction causing rainbow effect as seen in image (A) of Fig. 5.7. This can be explained by planes of quartz grain being fractured and causing light to bend as it passes through. Image B and C in Fig. 5.7 show similar grains observed through polarization. Both have fractured surfaces, which are caused by pressure from impact. Fig. 5.7 (D) shows yet another grain which refracts light, where each streak of purple is a separate fracture.

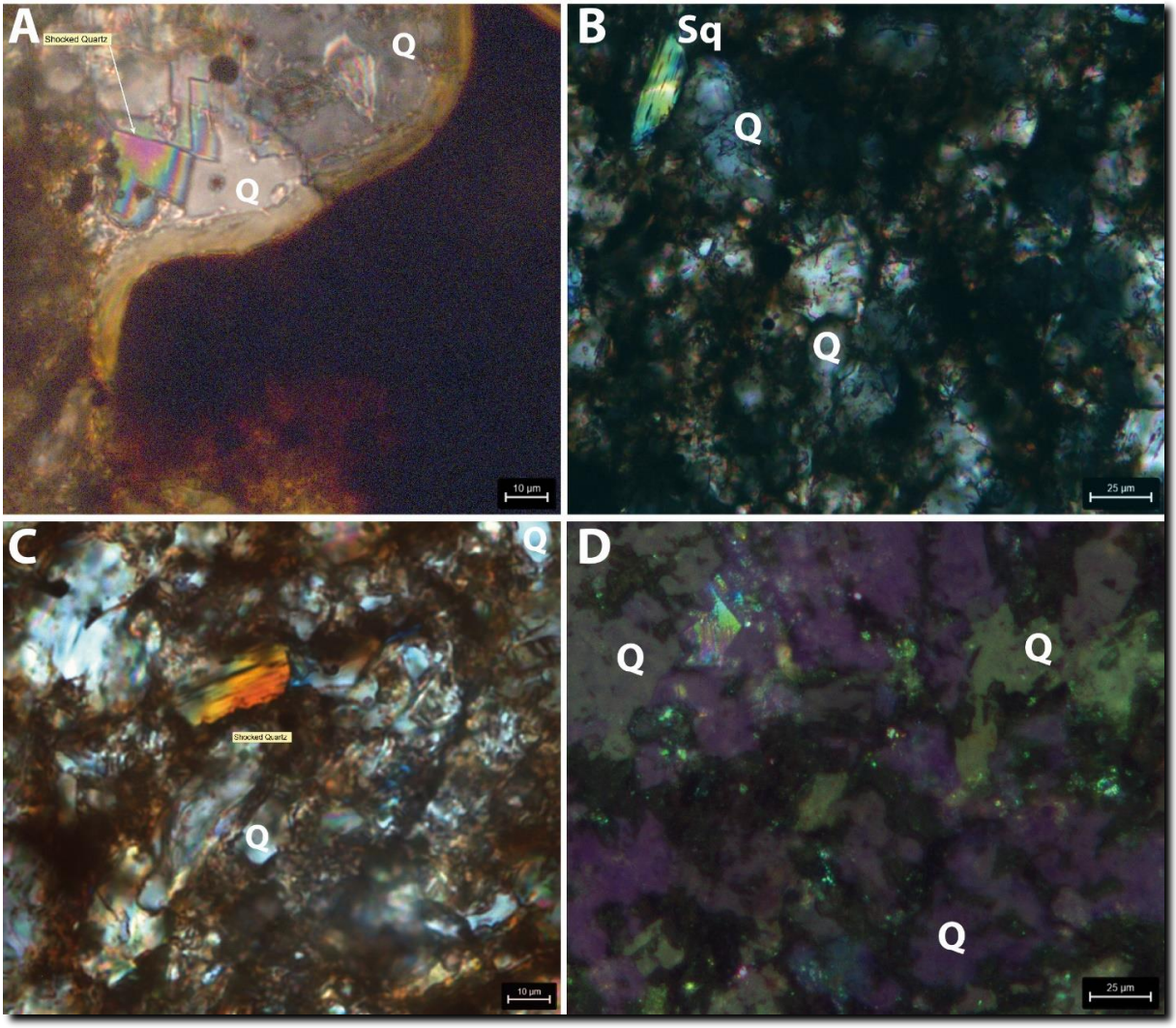

Fig. 5.7 *Examples of possible shock metamorphism in quartz grains from thin section 1.*

Interpretation

The features shown in Fig. 5.7 can only be explained as shock metamorphism of quartz. The refractive coloration in Fig. 5.7 (A) and (D) suggests that these could be Planar Deformation Features (PDFs), which are typically found in quartz grains related to bolide impacts (Goltrant et al., 1991). The possible implication of these grains is discussed later.

5.4 Scan Electron Microscopy

Use of SEM allows for in depth analysis of the various shapes microtektites can take, morphological features that may be found on their surface, and their internal structure and composition giving clues how they form. Multiple grains have been analyzed and scanned with Energy-Dispersive Detector (EDS), revealing the composition of the microtektites. Interestingly, the majority of spherules contain Aluminum (Al), Carbon (C), Iron (Fe), Oxygen (O) and Silica (Si) with occasional variations of some minor elements like Sulfur (S) for example. Iridium presence detected, but not in large enough concentrations to be seen as a trace.

Shape

Description

Microtektites observed come in four different shapes (Fig. 5.8). Many of the analyzed grains are very well-rounded spheres, while less common are oval grains like in Fig. 5.8 (A, B), tear dropped-like grains (C), or even drumstick-shaped grains (D).

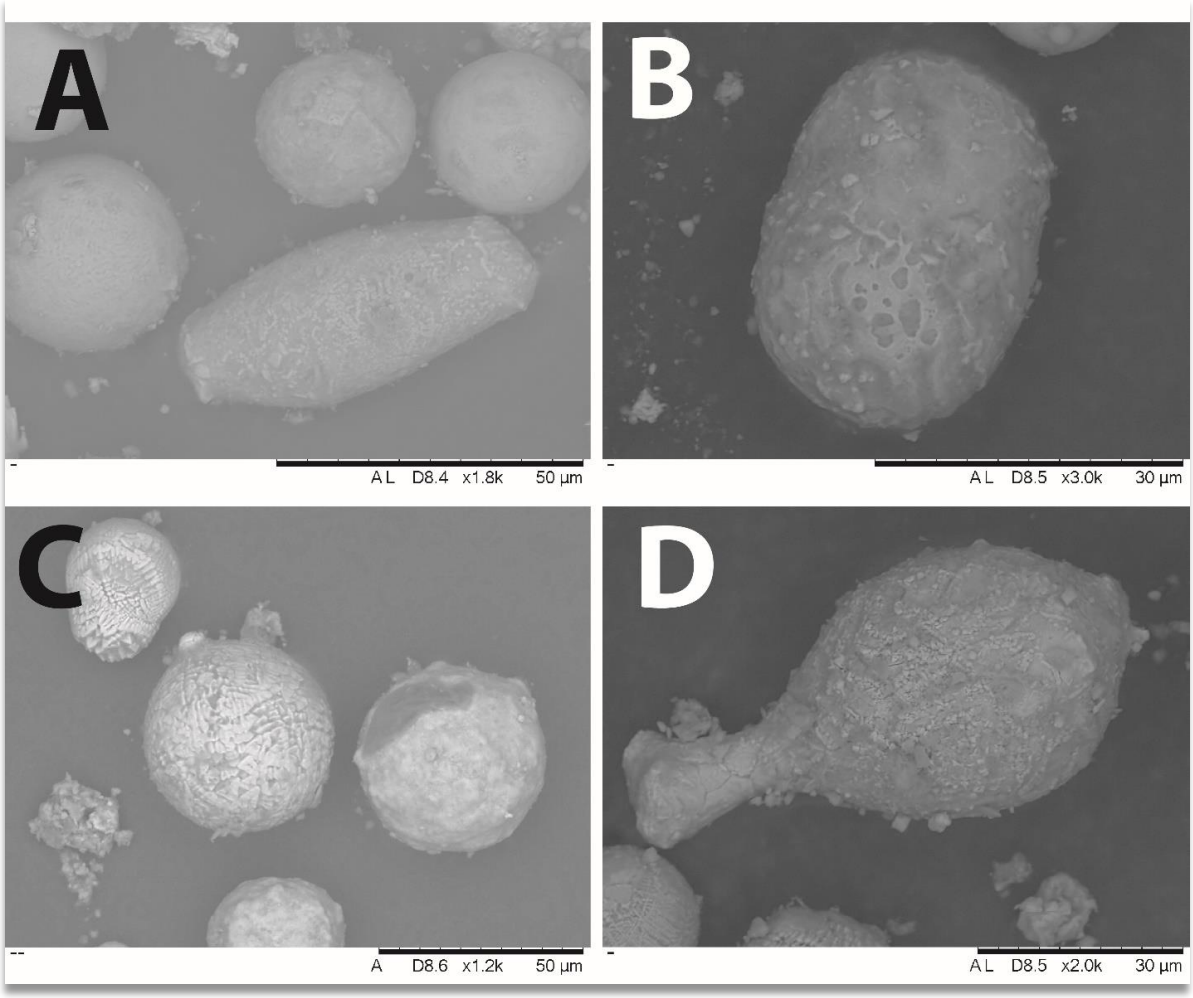

Fig. 5.8 *Shapes found within microtektite clusters. Spheres are common while the rest are uncommon for this sample.*

Interpretation

Shapes are entirely dependent on travel time of particles during re-entry. Spherules stay airborne longer and can keep their shape, while particle which are heavier due to possible fusion of two spheres fall faster and with help of gravity their shape is elongated sometimes having an oval appearance and other times look like a dumbbell (Claeys & Casier, 1994).

Texture

Description

When microtektites are seen through a regular microscope, they seem to be perfectly smooth. Once put through SEM, the true texture of these dust-sized particles is revealed. At higher magnification, more detail can be seen, for example various texture on their surface. Fig. 5.9 shows the wide variety of surface features (i.e. lineation and patterns) that can be seen. Composition-wise, they are all iron oxides except the one shown in Fig. 5.9 H which is a silicon dioxide. Size-wise, the mikrotektites ranges 5 – 10 µm and up to 300 – 400 µm. This range of sizes gives possibilities for varying degree of surface features to exist. Most striking morphologies appear in the smaller tektites from 5 up to 50 µm. 100 µm and above surfaces start to take more of a smooth look but still host countless fractures.

Interpretation

While falling through the atmosphere, spherules go through changes internally and externally. All the textures described here can thus be attributed to how fast or slow a droplet was falling and cooling. The intricate surface features are a combination of atmospheric processes such as friction and rapid cooling, causing dendritic formations of magnetite (Batovrin et al., 2021) (Fig 5.8). None of the textures seems to be related to post-depositional fracturing. Most tektites are highly magnetic. Magnetite and hematite and other iron oxides could be behind their compositional makeup.

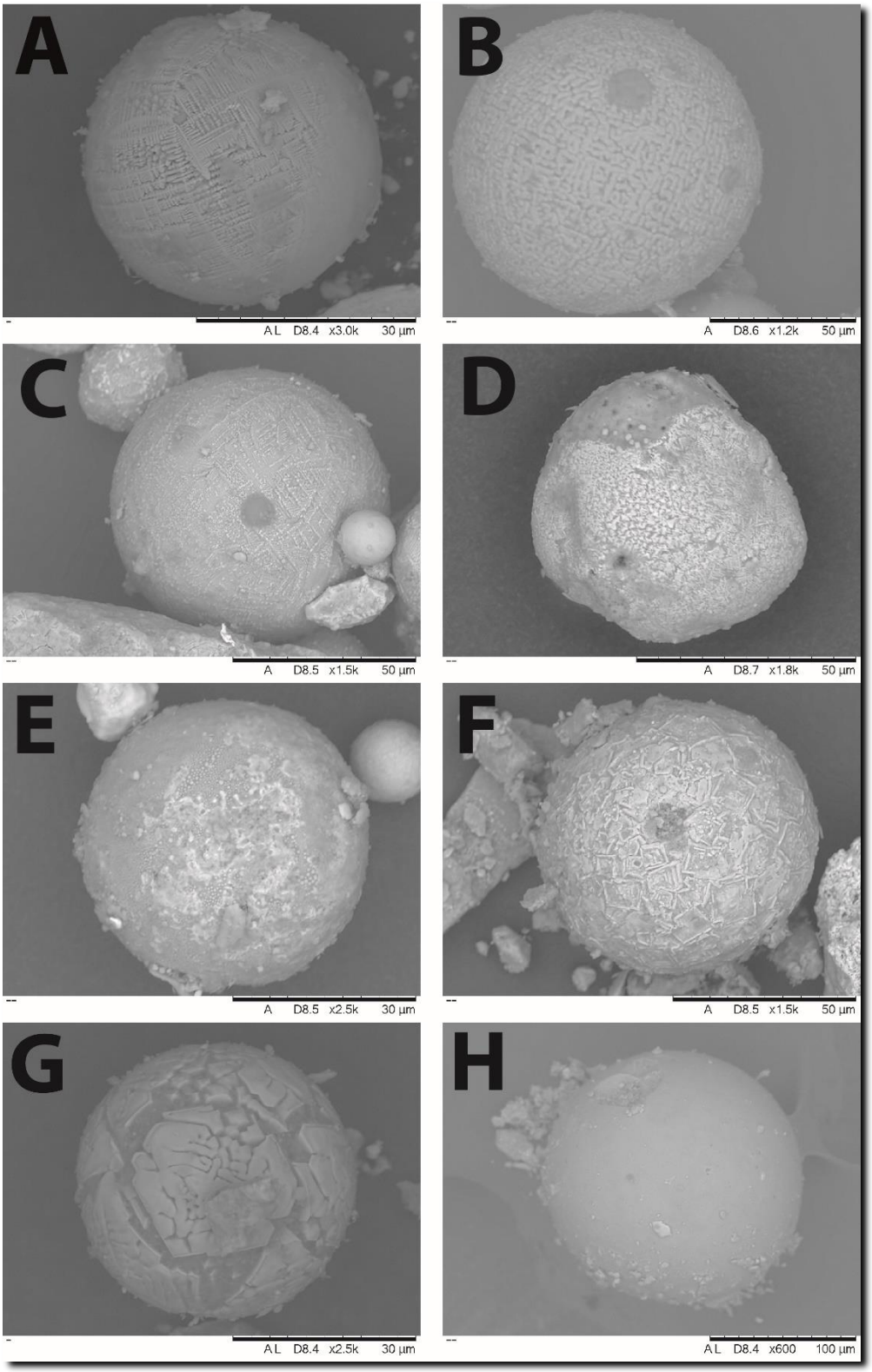

Fig. 5.9 *Surface textures recognized in microtektites from the New Albany Black Shale unit investigated here. Pictures (A) – (G) are microtektites of iron oxide composition and (H) is a glass spherule.*

Internal structure

Description

The investigated mikrotektites are just as impressive from the inside as much as outside. Fig. 5.10 shows fragments of various mikrotektite-shells, some possibly belonging to the same mikrotektite. Six of the mikrotektite fragments are relatively big between 100 – 300 µm.

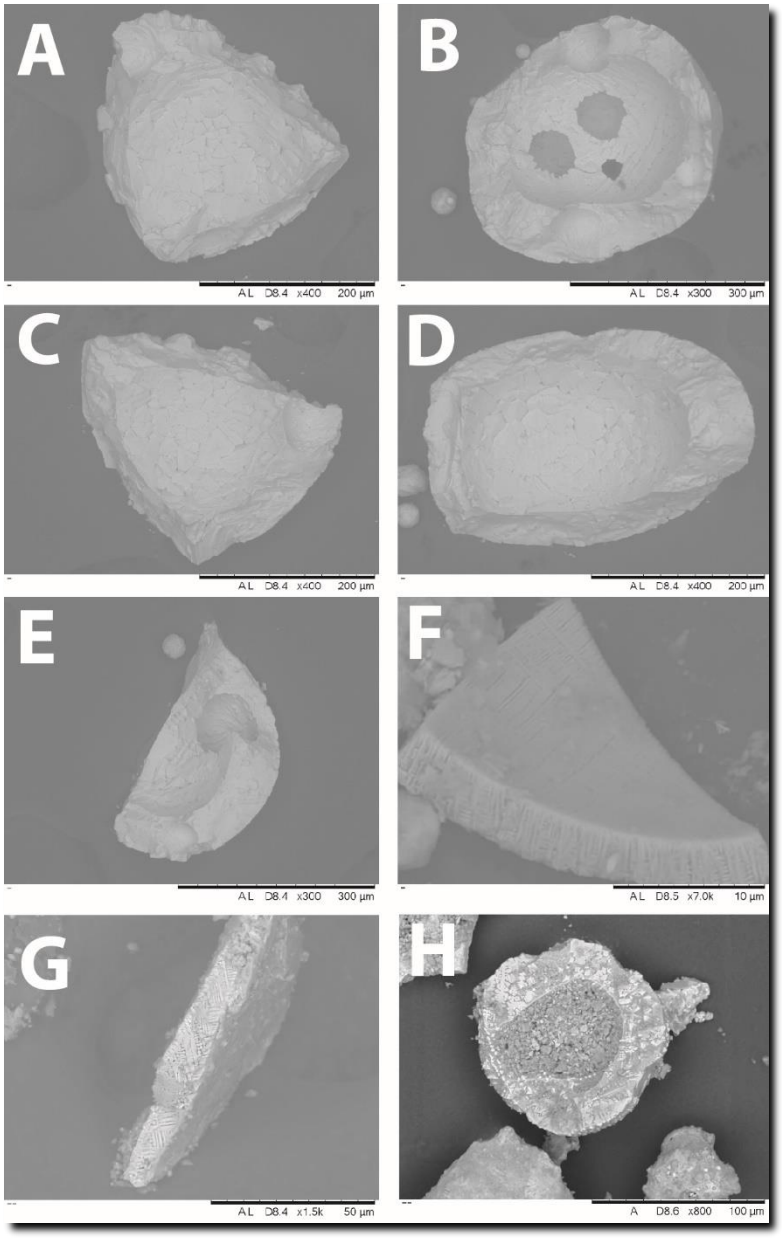

Fig. 5.10 *Images showing internal view of microtektite shell fragments featuring vesicles from gas escape, dendritic formations and linearly and cross cutting arranged grains.*

Interpretation

Images in Fig. 5.10 (A) through (F) show smooth internal walls with only difference in (F) featuring well developed columns laterally. This can be because of the spherule had a gradual cooling which gave time for crystals to arrange themselves neatly, or it could be a secondary shell formed atop of primary spherule while (A – E) appear to have cooled off quickly or instantly which causes vesicles of escaping gasses to form clearly visible within the shell and grain randomization (Shao et al., 2020). Image G and H both show dendritic arrangements of an iron oxide, like magnetite.

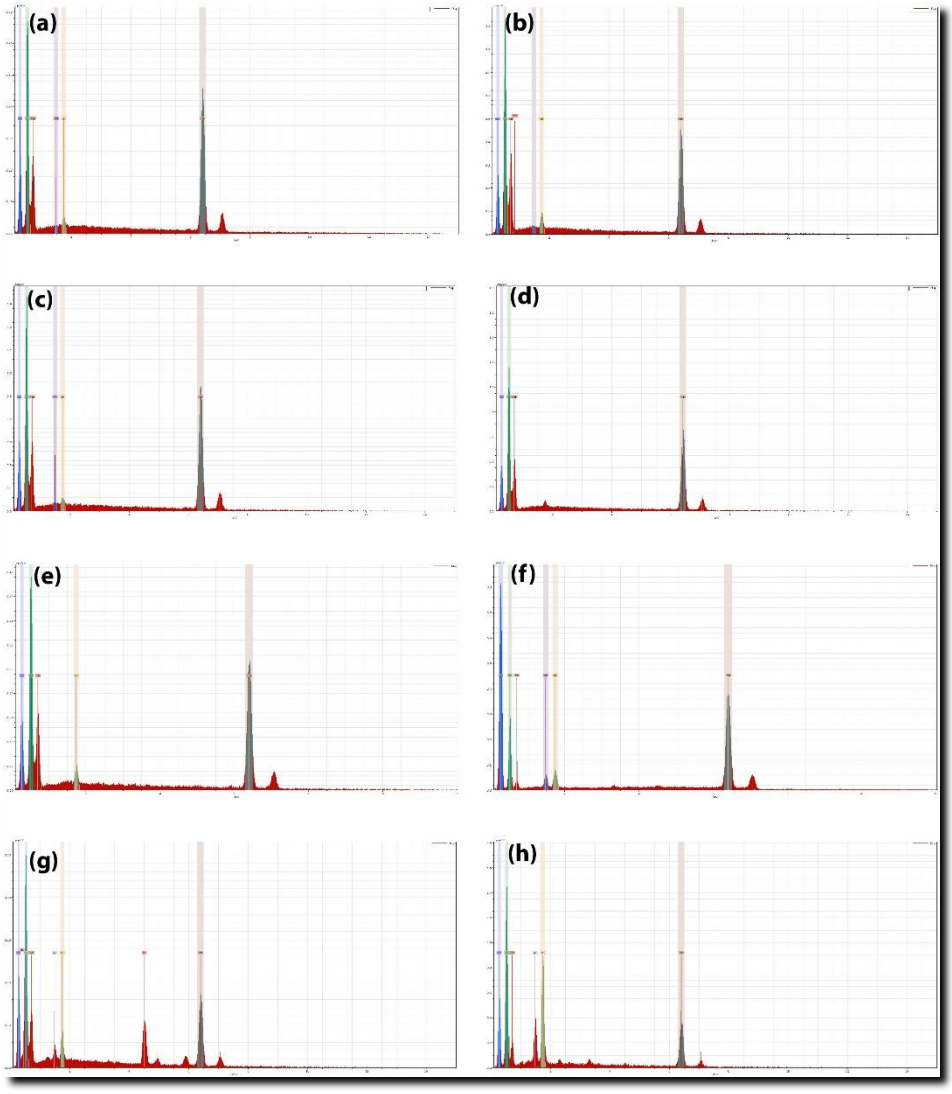

Fig. 5.11 *Elements found within shell fragments of Fig. 5.10. All are forms of iron oxide. G) contains traces of Titanium.*

Composition

Description

Overall composition of the microtektites is of the iron oxide group with occasional silica beads in the mixture. Through EDS analysis, elemental readings show 5 major elements found through all spherules that have been looked at (Fig. 5.11). The elements are Aluminum (Al), Carbon (C), Iron (Fe), Oxygen (O) and Silicon (Si). Occasional minor peaks of secondary elements have been spotted like Bromine (Br), Iridium (Ir), Potassium (K), Sodium (Na), Titanium (Ti) and Zink (Zn).

Interpretation

The importance of microtektite composition is that can help understand the lithology of possible rock types which were the source of the material that got ejected into the atmosphere. Based on the elements found in the studied grains. Based on the elemental composition of the analyzed spherules, a possible source could be an igneous rock due to the increased levels of oxygen and silicon while being overlain by some sediments which result in the carbon readings.

Classification of mikrotektites

Based on the above, 3 categories of mikrotektites can be recognized (summarized in Table 1 and Fig. 5.12). Type 1 mikrotektites are ranging from 5 μm in thin section 1 up to 200 μm in grains from carbon stub analysis, exhibit spherical and well-rounded shapes and a variety of textures, and consists of iron oxides with some additional elements. Big portion of microtektites is spherical and occur in assemblages along with pyrite framboids in a quartz dominated layer in thin section 1, although solitary grains have been documented in organic rich laminae as well. Type 2 range from 20-500 μm, having ellipsoid shape, very few specimens are found, composition is like Type 1. Their shape is contributed to spinning and gravitational forces during fall. Type 3, ranging from 30 μm to 60 μm is just as rare as Type 2 and compositionally the same as the res. The shape of a teardrop is formed when Type 2 splits apart from the rapid spin. The generalized categorizes defined here represent microtektites of slightly different origins or depositional time. Type 1, based on their shape and texture, must have cooled rapidly during entry. Type 2 have elongated or oval shape because some droplets began to spin mid fall

and gravitational forces pulled side to side giving it that shape. Type 3 is the product of an ellipsoid splitting in two due to its fast spinning.

Table 1. Summary of the microtektite classes defined in this study.

Class	Shape and size	Texture	Internal structure	Composition	Interpretation
Type 1	Well-rounded Diameter: 5 – 200 µm	Ridged, pitted, frosted	Solid or hollow. If hollow, cavity can be replaced with secondary minerals	Iron oxides with some silica	Rapid cooling during atmospheric entry
Type 2	Oval/ellipsoid Diameter: 20 – 500 µm	Linear, bumpy	Solid, May contain vesicles.	Iron oxides with some silica, potassium	Spinning and thumbling during entry
Type 3	Tear drops. Diameter: 30 – 60 µm	Ridged, rough angular	Solid	Iron oxides	Formed from the breakup of an ellipsoid due to centrifugal forces during spinning

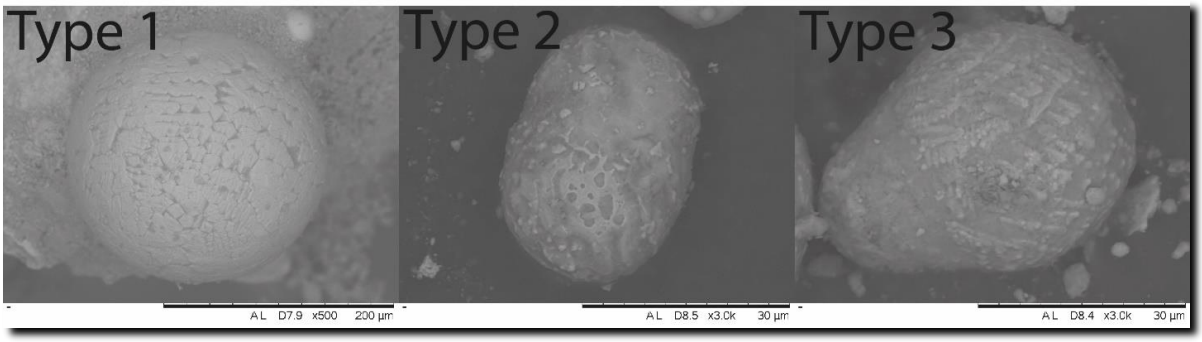

Fig. 5.12 *Examples of microtektites from each type.*

6 Discussion

Based on the analysis presented in this thesis, there are several results pointing towards an impact, including the presence of microtektites, many with compositions and textures conforming to impact-related tektites elsewhere. However, globally, there are many reports of Upper Devonian sections recording evidence of widespread anoxia. As such, the first part of this discussion focuses on the microtektites and their potential of being proxies for an impact, whereas the second part deals with known causes of anoxia and their potential link to the Late Devonian mass extinction.

6.1 Age of the Frasnian-Famennian (FF) boundary and the Late Devonian mass extinction

To provide a sound and reasonable discussion of potential causal factors driving the mass extinction, a summary of the suggested ages of the mass extinction, as well as the associated FF boundary interval is given here. In discussing global events, particular mass extinctions, similar-aged and correlatable sections is crucial. Several ages have been proposed for the Late Devonian event, first of which was set at 376 ± 3 Ma (Courtillot et al., 2010), thereafter a new study calibrated the date to 372.36 ± 0.053 (Percival et al., 2018). The present geological time scale (Cohen et al., 2023) places the FF boundary at 372.2 ± 2 Ma.

6.2 Microtektites - evidence of an impact?

The presence of microtektites and their composition and textures have been explored in this project (Figs. 5.4, 5.5 and 5.9). The investigated samples derive from an outcrop of organic

rich, black shale that was deposited in the Illinois Basin (USA), which was a partly landlocked and anoxic basin during the Late Devonian. The intriguing results from the analyses presented here, clearly demonstrate the presence of various microtektites and thus provides a new, additional strewn field complementing the Hony and Senzeille sections in Belgium, and the Qidong section in China (Claeys & Casier, 1994). Thin sections and collected material have been analyzed through few methods to test the legitimacy of the dust-sized spherules (see Method chapter). Out of four thin sections, three were heavily laminated, pyrite-bearing, and rich in organic matter (OM), while the last one was entirely made of quartz (heavily cemented). The OM rich thin sections show sparse pyrite in the forms of single grains, and rarely in the typical large framboids that many black shales are known for. Nonetheless, all the features combined indicate deposition in an oxygen-deficient, stagnant environment below storm wave base. An interesting occurrence was noticed in thin section 1, where assemblages of pyrites and microtektites have been observed, while in the other sections, no such linked assemblages were found. One possible explanation is a 'seeding period' where the microtektites which eventually fell out of suspension and were deposited on the basin floor, introduced iron molecules to the sediment. In the meantime, the water column is teaming with sulfate-reducing bacteria which releases sulphide that eventually ends up reacting with the iron molecules to form pyrite (Duverger et al., 2020).

When thin section 1 was analyzed under a reflected light, pyrite showed up with the usual yellow hue, while microtektites did not. However, in thin section 3, a handful of microtektites appeared under reflected light. This begged the question what these tiny spherules were really made of, and why they show up in some instances and in others not. Microtektites were therefore extracted and placed on carbon stubs which were analyzed using Scan Electron Microscope (SEM) equipped with Energy Dispersive Spectrometer (EDS). Compositionally the microtektites are a form of iron oxide with some other accessory elements. They are generally highly magnetic which could be due the presence of magnetite, which is a form of iron oxide. Occasionally some silica oxides are also seen, therefore it is safe to conclude that these spheres do have a wide range of compositions, which may give them unique properties such as isotropy (Claeys et al., 1992) under polarized light and sometime being reflective under reflected light. The overall composition revolves around five elements: Aluminum (Al), Carbon (C), Iron (Fe), Oxygen (O) and Silicon (Si) (see Fig. 5.9 and 5.11). Besides composition, SEM analysis was able to give an insight of the morphologies of the grains. The spherules come in a

wide range of sizes with some of the smallest ones recorded being under 10 µm and going up to 500 µm. Their size in some way dictates the shape, while air friction and cooling during fall dictate surface features they would have. Both of which are decided in midair during reentry into Earth's atmosphere. For instance, if a microtektite is on the larger side, during flight it may start spinning fast to the point where centrifugal forces split it in half which would produce two grains with a tear drop shape. Some other forms besides tear drops, include the typical well-rounded spheres as well as ellipsoids which are not fully formed dumbbells (Fig. 5.12). If the microtektite is an iron oxide like the ones in Fig. 5.9, most of the time they would form complex surface features like pits, ridges or frosted snowflake looks. If a spherule is made of silica, however, no impressive surface features are present (see example in Fig. 5.9 H). What type of surface features that develop, are entirely up to how quickly the grain falls and cools down since crystallization is dependent on time. Fast falling grains would result in fine crystallization, whereas slow gradual falling would result in the formation of well-defined crystals or even complex surface features (see contrasting examples in Fig. 5.9 D and 5.9 G)

When investigating microtektites, one important question arises: where are they coming from? Luckily, based on composition, size, and shape, some educated guesses can be made. According to Glass & Simonson (2012), microscopic ejecta debris from the Chicxhulub crater in Mexico, microtektites were found in a 5000 km radius, while the smaller and associated microkrystites were found around the globe. When this is taken into consideration and given the fact that the spherules documented in this project are most likely microkrystites, which are darker and far smaller than microtektites, which are generally larger and mostly felsic, it is safe to assume that wherever the responsible impact happened, it was very far away from the Illinois Basin. A potential impact could be the Woodleigh structure in western Australia, since it sits roughly within the same paleo-latitude as Qidong (China), Hony and Senzeilles (Belgium), and more interestingly, the Illinois Basin (USA) investigated here. Thus, with the Coriolis force and the planet's spin taken into consideration (Xu et al., 2023), dust-sized debris would be able to reach all these locations sometime after a potential impact. When it comes to volcanics, no active volcanoes were present in the vicinity of the Illinois Basin, and volcanoes do not typically produce microtektites of the types described here. As such, it is clear, based on their compositions and textures, that the spherules are in fact proper, impact-related dust-sized, micro debris. However, due to the lack of stratigraphic evidence of microtektites from other Upper Devonian sections across the globe (apart from Belgium, China, and now also USA), the

amount of data is not enough to establish a solid argument that a massive impact occurred and was the main cause of the mass extinction. Instead, one or several smaller entries and impacts seems more likely, potentially contributing to the already ongoing crisis (Percival et al., 2018). Therefore, other mechanisms were more likely to be the main causes of the extinction, including volcanism, anoxia, and climate changes, as discussed below.

6.3 Volcanic activity

Volcanic activity, and particularly the emplacement of Large Igneous Provinces (LIPs), has the potential to coat the planet's atmosphere in a thick layer of ash that could render the planet from receiving heat from the sun, including the release of poisonous gasses that can affect the Earth's Systems (Ricci et a., 2013). Several other mass extinctions and hyperthermals have been linked to LIP emplacement, including the well-studied end-Permian event where the Siberian Traps stands out as a primary cause (e.g. Zuchuat et al., 2020). Mercury (Hg) anomalies, which is commonly taken for a proxy of intense volcanic activity (e.g. Jones et al., 2023), have been documented in multiple Upper Devonian basins (Rakocinski et al., 2020). Rakocinski et al. (2020), proposed that Late Devonian climatic changes were the cause for the oceans to turn anoxic and lead to the mass extinction, but further suggested that for those changes to take place, something of cosmic or LIP proportions had to have occurred first. It has been suggested that extensive magmatic and associated hydrothermal activity took place at the end of the Devonian, as evidenced by high concentrations of Hg documented in Upper Devonian sections in Italy and Austria, as well as the presence of Late Devonian LIPs around the globe (Rakocinski et al., 2020). Barash (2017), for example, suggests that Late Devonian volcanism in the Viluy Trap province (Siberia, Russia) may have played a major role in the mass extinction due to its vast size, covering most of present-day central Russia.

Mercury (Hg) anomalies have been widely accepted as the proxy directly linked to volcanic activity such as LIPs (Racki et al., 2018; Jones et al., 2023). These anomalies usually appear on a global scale, like in Upper Devonian sections in the Lahmida (Morocco), Kahlleite (Germany), and the Ural Mountains (Russia) all of which represent the FF boundary (Racki et al.,2018). Racki et al. (2018), argues that although there are multiple LIPs occurring at the time of the Late Devonian extinction, none of them happen at the exact time of the Frasnian-Famennian boundary interval (i.e. c. 372.2 Ma), furthermore, it is suggested that the geochronological methods used to date each LIP have to be improved to get a more accurate

dating. The three locations mentioned above indicate increased levels of Hg. All anomalies were found throughout the entire Frasnian-Famennian boundary interval and in different lithologies, suggesting that the Hg is not only related to black shales deposited under anoxic conditions. Instead, these anomalies can be seen as a sign of a continuous volcanism that could have lasted for >100 kyr as seen in Hg-enriched horizons in the Upper Devonian of the Ural Mountains (Racki et al., 2018). Center Hill (USA) host Upper Devonian strata and record a Hg anomaly that has been recorded worldwide, corresponding to the Upper Kellwasser event (Racki, 2020). This signal is believed to be the combined result of all major LIPs worldwide to show same pulse patterns, which would explain the anoxia and Hg enrichment seen across more or less the same time horizonaround the globe (Racki, 2020). Rakocinski et al. (2020), suggests that the high concentration of Hg in places like Austria and Italy are due to pulses from one of the major Russian LIPs, either being the Siberian, Kola, Pripyat or Magdalen (North America) LIPs.

Volcanoes introduce or have introduced most of the Hg present on the planet's surface. The bulk of the Hg is in a gaseous state and can linger in the atmosphere for over a year. When there are high global concentrations of Hg in time-equivalent strata, this strongly suggests that LIP was the catalyst, further indicating that the amount released during such an event is far greater than what the land, ocean, and organic matter collectively can absorb. If anomalies are more local, for example confined only to a single basin, that imply that either small scale hydrothermal activity was present or it can be the product of wildfires and erosion, which can bring sediments rich in Hg into the basin (Zhang et al., 2021). The sudden Hg-bearing sediment load transported to the sea floor from an eruption, causes oxygen to be used in oxidation processes, which in turn depletes the water column of oxygen and allows for sulfate reducing bacteria to begin digesting the gas form of mercury and transform it into its more potent and volatile form: methylmercury (MeHg) (Rakocinski et al., 2020), see Fig. 6.1. This form is naturally attracted to carbon based organic matter (which also explain why Hg is commonly associated with organic-rich, black shales) and the affected ecosystems soon starts to feel the severe effects of this strong neurotoxin once it makes its way into the water column (Rakocinski et al.,2020).

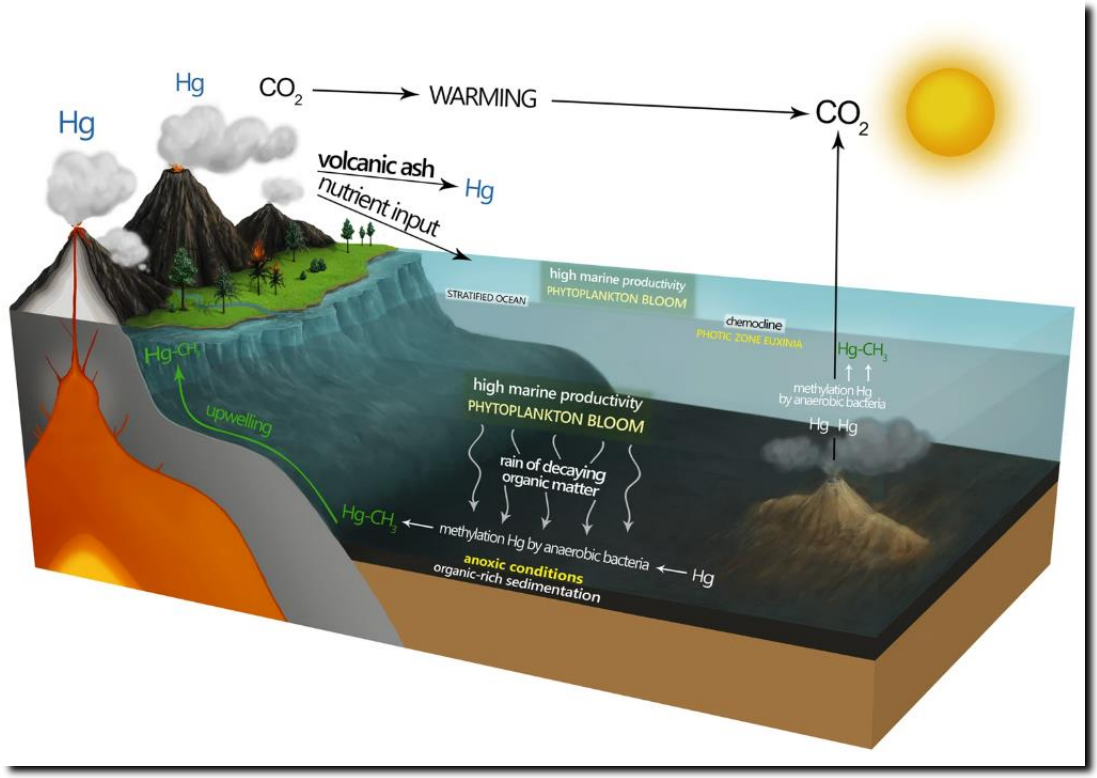

Fig. 6.1 *Methylmercury cycle, starting from eruption to release of mercury gas into the atmosphere and then being absorbed into the ocean and transformed into a solid by bacteria. From Rackocinski et al. (2020)*

Zheng et al. (2023), challenge the idea of volcanism and Hg influx as a trigger to the Late Devonian extinction, because studies across the globe show that Hg is found in stratigraphic sections of various lithological compositions, and which are located far from any volcanic provinces. Furthermore, it has been suggested that Hg can be provided and accumulate by other means such as soil erosion, anoxic processes in oceans (caused by other processes such as water column stratification), and wildfires.

Various workers have tried to resolve the question regarding when exactly the Siberian LIP has been active. The so-called Viluy Trap is a part of triple junction rift of the Siberian LIP which is currently being debated whether it influenced the Frasnian-Famennian boundary interval. Many suggest that the Viluy Traps (central Siberia, Russia; Fig. 6.3) have been a subject to multiphase magmatic events which occurred at different times separated by millions of years. One such example of a study comes from Courtillot et al. (2010), where two sets of plagioclases were subjected to analyses from two laboratories operating with different methods of determining ages. One used potassium (K) – argon (Ar) method and estimated age was 338

± 4.8 to 352.8 ± 5 Ma. Second lab based its analysis on $^{40}Ar/^{39}Ar$ and concluded with a range of 370 ± 0.7 to 373.4 ± 0.7 Ma see Fig. 6.2.

Sample	Plateau age (Ma)	Integrated age (Ma)	K-Ar age (Ma)	Decay Constant
30/01	370.0±0.7	367.0±2.0	367.2±5.2	Steiger and Jäger (1977)
	373.4±0.7	370.4±2.0	370.3±5.3	Renne et al. (2010)
35b/01	none	344.3±1.9	342.4±4.9	Steiger and Jäger (1977)
	none	347.5±1.9	345.3±5.0	Renne et al. (2010)
42/01	none	349.4±1.9	338.0±4.8	Steiger and Jäger (1977)
	none	352.6±1.9	340.9±4.9	Renne et al. (2010)
42a/01	359.9±1.9	356.0±2.0	352.8±5.0	Steiger and Jäger (1977)
	363.2±2.0	359.3±2.0	355.8±5.1	Renne et al. (2010)

Fig. 6.2 *Age comparison of Argon dating versus Potassium dating of the Viluy Trap. From Courtillot et al. (2010).*

Difference in ages can be explained by the volume of gasses left in samples at the time of testing. As a result, Courtillot et al. (2010), proposed that even though the Viluy Trap was last active 370 Ma, the main phase of eruptions was subsequent to the Frasnian-Famennian boundary (372.2 ± 2 Ma), and therefore played no direct role into the Late Devonian extinction.

Contrary to Courtillot et al. (2010), Ricci et al. (2013) suggests that there is a correlation between continental flood basalts (CFB) and oceanic anoxia, with the impressive amount of up to 10 million km^3 of material deposited within a 10 million km^2 area occurring in three out of five mass extinctions within the Phanerozoic with the potential of adding the Late Devonian as the fourth by looking into Viluy Traps. Furthermore Ricci et al. (2013) suggests that the Siberian Traps have been linked as having a direct effect on the environment following intense periods of volcanic activity. Thus, CFBs of these proportions can be related to LIPs which have negative effects on ecosystems, such as the Siberian LIP. LIPs have a history of being connected to extinctions such as K-T, Tr-J and Permian-Triassic boundaries.

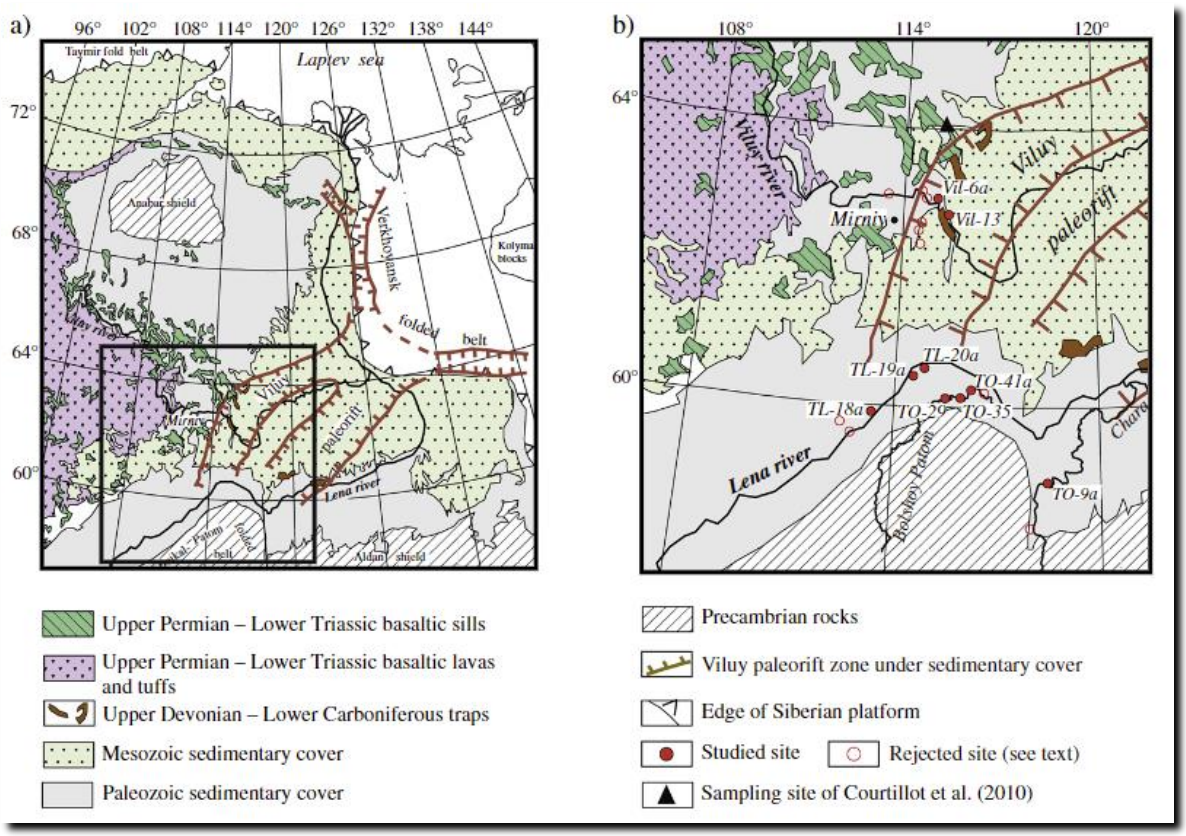

Fig. 6.3 *A) overall structure of Siberian LIP, B) inset of study area and sample collection sites. From Ricci et al. (2013)*

Ricci et al. (2013) suggested that the Viluy Trap, was part of the Siberian LIP during the Late Devonian, which was a triple junction rift system, at least being up to 800 km long and 450 km wide. Old volcanic rocks can be seen at the edges of the preserved rift structure, and the central part is covered by a thick succession of sedimentary rocks with an estimated thickness of up to 8 km. The volume of basalt released is speculated to be around 300 000 km^3. Through the study of 9 rock samples picked from various localities within the reach of Viluy Trap, with the use of $^{40}Ar/^{39}Ar$ method, it was concluded that this part of the triple junction has experienced multiphase volcanism with two main events dated at 376.7 ± 1.7 and 364.4 ± 1.7 Ma. At the time of the study the FF boundary age was set at 376.1 ± 3.6 Ma (presently set at 372.2 ± 1.8 Ma). With that date in mind, it is accepted that the first volcanic phase at 376.7 ± 1.7 Ma may have played a role in the mass extinction associated with the FF boundary (see Fig. 6.4).Ricci et al. (2013), further supports the potential of intense volcanism by arguing that all other proposed models for the cause of anoxic conditions during the Late Devonian barely hold any ground, including suggestions of marine regression and transgression, massive erosional events

which would add a heavy sediment load into the water mass, or the massive and sudden boom of flora on land.

The prospect of an impact is also challenged and found highly unlikely because there are no iridium anomalies identified yet or anything else to suggest that an impact may have been the cause (Glass & Simonson, 2012; Ricci et al., 2013). The impact crater being closest in time to the FF boundary is the Siljan Ring impact in Sweden, but it has been disregarded as being too small of an impact to bring cataclysmic consequences on a global scale (Ricci et al., 2013).

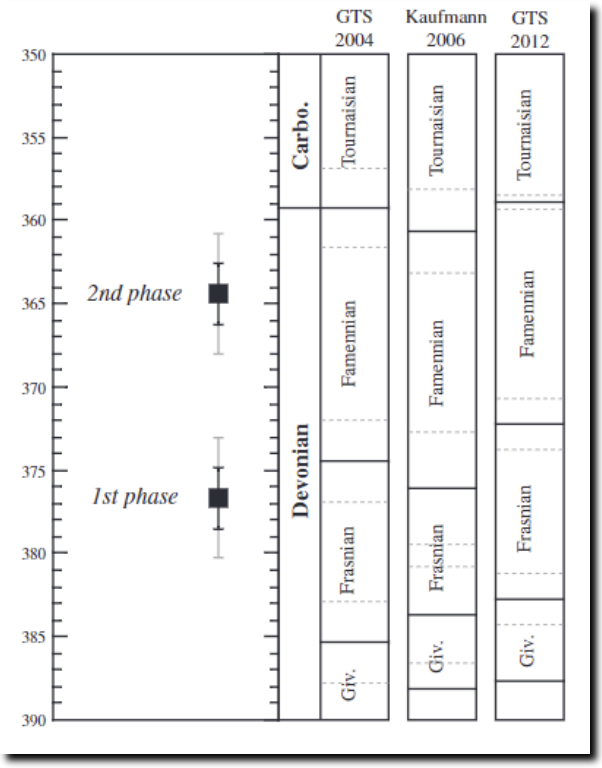

Fig. 6.4 $^{40}Ar/^{39}Ar$ average ages of the two Viluy Trap episodes along with most recent for the time proposed ages of the FF boundary. From Ricci et al. (2013).

Percival et al. (2018), employed the U/Pb method of dating and looking at zircon crystals extracted from aluminum phyllosilicate clay or bentonite. They determined that the average age of all samples gathered from a quarry in Germany analyzed was 372.36 ± 0.053 Ma which would give the most accurate and up to date age of FF boundary. Because of the new age of FF boundary and previous works in the sphere of the Viluy Traps, Percival et al. (2018), terminates

the possibility of the two Viluy Traps episodes to be linked in any way to the boundary, simply because the first episode occurred during the late Frasnian at 376.7 ± 1.7 Ma and the second episode happened in the late Famennian at 374.1 ± 3.5 Ma (see Fig. 6.5).

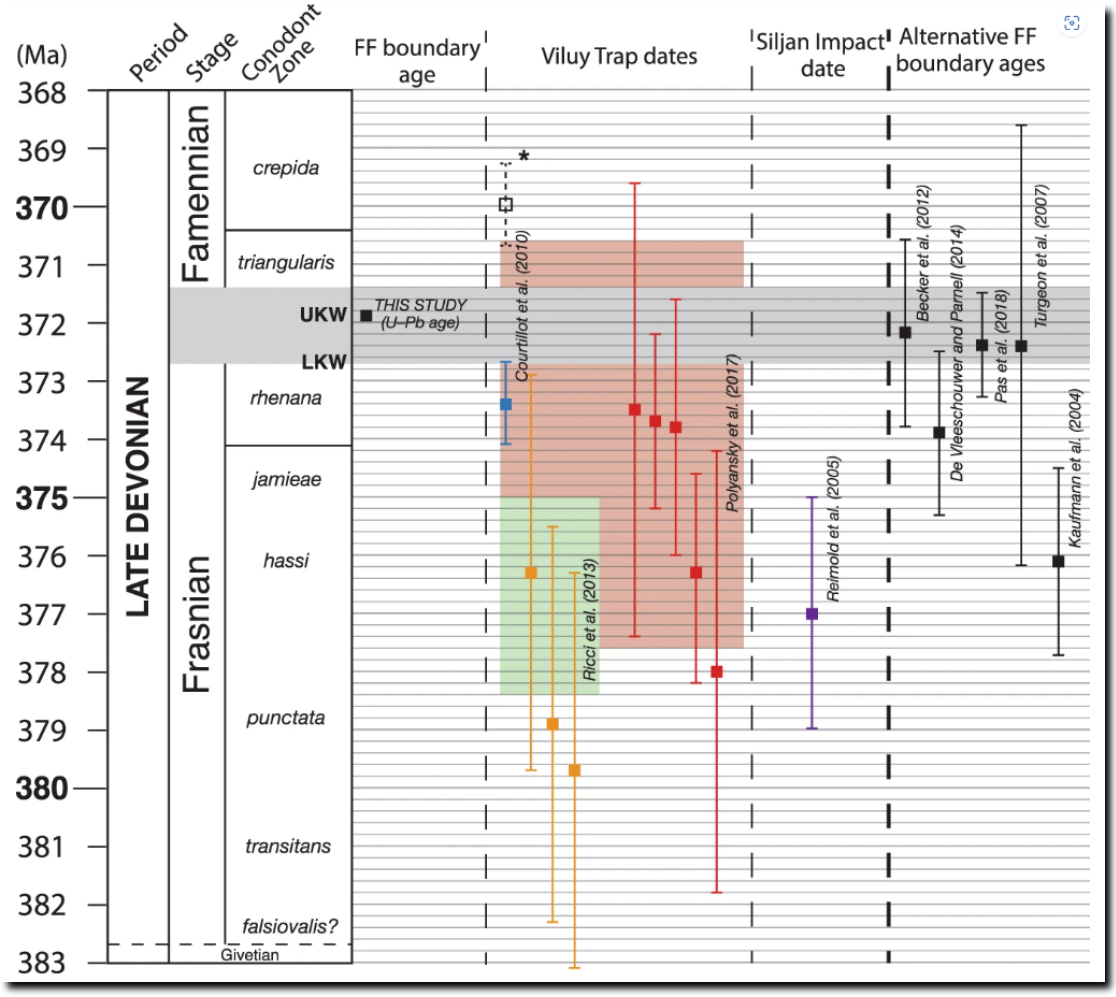

Fig. 6.5 *Most recent FF boundary dating in comparison to previous Viluy Trap dates and previous FF boundary dates. From Percival et al. (2018).*

Other Devonian LIPs that have been proposed as drivers of the extinction are the Pripyat-Dnieper-Donets (PDD) LIP, and the Kola LIP (Bond & Wignall, 2014). The PDD LIP doesn't really qualify and should be rejected as a cause because of the little volume of lava released and its activity seems to be centered around 367-364 Ma (Famennian), making it younger. The Kola LIP is neither considered, because it is much older than the FF boundary, aged at 380-375 Ma (Bond & Wignall, 2014). Lastly the Magdalen LIP (USA/Canada), which was emplaced in Laurentia during the Late Devonian, has been speculated to have been active between 380-360 Ma, but due to lack of precise dating an absolute link with FF boundary hasn't been achieved

yet (Ernst et al.2020). For the time being, neither volcanism nor impacts have been dated to the time of the extinction at 372.2 Ma, albeit volcanism linger as the strongest candidate with multiple pulses before and immediately after the FF boundary interval.

6.4 Greenhouse, icehouse and evolution of vegetation

Abrupt and severe climatic changes have been investigated as another possibility that would have led to the mass extinction in the Late Devonian. A geologically rapid transition from a warm and humid climate to cooler and dryer one can theoretically bring the biosphere to a collapse if it is faster than the time needed for the biosphere to adopt. Climate is a complex system that is governed by things like volcanism responsible for CO_2 emissions, which in turn increase Earth's temperature over time leading to greenhouse effect, vegetation, which if present, regulates CO_2 and thus the temperature. Oxygen levels up to the Late Devonian were low until a period of glaciation started to take a foothold (Tuite Jr et al.,2019). According to Tuite Jr et al. (2019), close to the FF boundary, CO_2 levels were at 1022 ppm and the end of the Famennian it apparently dropped to 590 ppm. A reason for this dramatic change may relate to the introduction of vascular vegetation on land. Once plants established themselves, their collective vast root system began to transform the former barren landmass into a massive carbon sink which in return caused the CO_2 levels to drop drastically. Another striking indication reported by Tuite Jr, et al. (2019) was the sudden rise of pH in the Late Devonian oceans. A rise like that can disrupt the Nitrogen (N) cycle, which is an important part of every living organism. During greenhouse conditions, CO_2 levels were high and O_2 and pH were low, leading to nitrification to take place, which is good for living organisms that rely on compound nitrogen as their primary food source. In contrast, icehouse conditions cause nitrification and denitrification to occur, which makes N to be stored in sediments instead of being absorbed by living organisms (Tuite Jr et al., 2019). Another effect of such transition is the relationship of global temperature and sea level. Speculated by McClung et al. (2013), a possible incremental icecap development may have happened during a major turnover from greenhouse to icehouse starting in the Middle Devonian and ending in the Late Devonian. Ice sheet formation would have lowered the eustatic sea level over time, which would increase sediment load due to exposure, fluvial incision and increased runoff into basins that experienced falling sea level, thus becoming more saturated with nutrients, and causing anoxic conditions due to oxygen depletion by the death and decay of organisms like the Tasmanites found in thin sections 2, 3 and 4 which form vast algal blooms.

6.5 Sources of error and future outlooks

Besides assemblages of pyrite and microtektites, another potential evidence of an impact is also present in the form of shock metamorphosed quartz in thin section 1. When the thin section is observed under cross polarized light, portion of the quartz grains light up in a rainbow fashion, which could indicate the presence of planar deformation features (PDFs) (Goltrant, Cordier & Doukhan, 1991). The possibility of shocked quartz would indeed solidify the bolide impact-theory, although a closer inspection is required to make sure that the observed features are in fact such a structural deformity. Another pitfall is of course the age of the inferred shocked quartz grains. Albeit they occur in Late Devonian strata, they could of course relate to a much older impact, thus being a result of sediment recycling and redeposition whereby the Illinois Basin acted the final sink for these grains. Given the limited amount of data analyzed in this thesis, a natural next step would be to check for the presence of microtektites in the stratigraphic units above and below the investigated Camp Run Member and try to constrain the intervals where they are most abundant. A more systematic approach would also be favorable, including sampling the entire New Albany Shale, and do a comprehensive XRF study (for detailed elemental composition, including mercury) combined with organic geochemistry (for total organic carbon and total sulfur contents), as well as isotope studies (organic carbon isotopes and mercury isotopes). Collectively, such an effort would aid in the recognition of various paleo-climatic signals and fluctuating oxygen conditions in the basin, as well as to detect potential volcanic signals (e.g., Hammer et al., 2019) and thus separate these from the intervals exhibiting impact signatures (i.e. microtektites etc.).

Conclusion

The mystery of the Late Devonian mass extinction, which occurred around the Frasnian-Famennian (FF) boundary interval (at c. 372.2 Ma) has yet to be solved. A multitude of different hypotheses/theories have been proposed, ranging from global magmatic activity related to the emplacement of large igneous provinces, rapid colonization by vascular land plants, algal blooms in the oceans eventually causing anoxia, as well as onset of glaciations that eventually lead up to the late Paleozoic Ice Age. This project has attempted to add a new and important piece to the big puzzle by petrographically investigate some Late Devonian-aged, organic rich, pyrite-bearing black shale samples from the Illinois Basin, USA, that contain microscopic, dust-sized debris, referred to as microtektites, which may originate from a potential bolide impact in the Late Devonian. The investigated samples are part of the New Albany Black Shale group more specifically the Camp Run Member, which is a unit of shale slightly younger than the FF boundary. By combining conventional petrographic analysis, X-Ray Fluorescence (XRF), X-Ray Diffraction (XRD), and Scanning Electron Microscopy (SEM) analyses, this study show the following:

- The investigated thin sections show that the shales contain abundant organic matter and pyrite, suggesting that the basin was characterized by periods of anoxia. However, Tasmanites algae occur in the investigated samples, indicating that the water column was not entirely oxygen deficient. It may thus be speculated that algal blooms and increased primary production contributed to anoxia, and not only the land-locked nature of the basin as previously proposed.
- The microtektites exhibit a wide range of sizes, textures, and compositions. In general, they are iron oxides with varying accessory elements. Their composition and texture collectively suggest that they are in fact impact ejecta (rather than a bi-product of volcanism), very much resembling similar dust-sized, impact-related debris reported elsewhere.
- Pyrite and microtektite assemblages occur in a quartz layer absent of organic matter. Both occur in proximity to one another, suggesting a probable seeding of iron molecules by the microtektites and subsequent pyrite formation.

- The shale is generally composed of quartz grains and subordinate micaceous grains. However, several grains exhibiting characteristics of shocked quartz (i.e. rainbow color, PDFs with vesicles.) have been detected in the investigated samples.
- Iridium was detected but not of significant amount to be seen as a trace.

Particles such as microtektites and shocked quartz have previously been proposed as evidence to rejuvenate the debate of the impact hypothesis. Thus, based on the above results, especially given the character of the microtektites and the recognition of potential shocked quartz grains strongly suggests that an impact occurred near the FF boundary. Spherules of this size can be derived by other means as well, such as volcanic activity, but there are not any known Late Devonian volcanics in the Illinois Basin or in the adjacent and nearby parts of Laurentia.

Finally, this project does not attempt to challenge the already proposed and established mechanisms that caused the Late Devonian mass extinction, but instead resurrect an old theory that has for long been disregarded as a possibility, mostly due to the limited number of locations that have preserved microscopic particles like the ones reported here. Maybe after all, the extinction was not caused by a single mechanism, but being the combined product of multiple cataclysms of global proportions, including intensive volcanic eruptions, temperature changes, disturbances in chemical cycles, and as argued here, cosmic impacts. The severe effects seemingly endured over a sustained period, to the point where the planet's eco-system eventually collapsed. Could it be that an impact spurred the crisis by driving the climate past its tipping point? The one who seeks shall find.

Appendix

Raw data is available upon request.

References

Abdi, Z., Rimmer, S. M., Rowe, H. D., & Nordeng, S. (2024). Trace-metal enrichment mechanisms in Bakken Formation black shales, Williston Basin, North Dakota, USA. *Chemical Geology*, **646**, 121892. Doi: 10.1016/j.chemgeo.2023.121892

Algeo, T. J., Lyons, T. W., Blakey, R. C., & Over, D. J. (2007). Hydrographic conditions of the Devono–Carboniferous North American Seaway inferred from sedimentary Mo–TOC relationships. *Palaeogeography, Palaeoclimatology, Palaeoecology*, **256**(3–4), 204–230. Doi: 10.1016/j.palaeo.2007.02.035

Algeo, T. J., Shen, J. (2023). Theory and classification of mass extinction causation. *National Science Review*, **11**, 1 – 9. Doi: 10.1093/nsr/nwad237

Alvarez, W. (1994). Trajectories of Ballistic Impact Ejecta on a Rotating Earth. Abstracts of Papers Presented to "*New Developments Regarding the KT Event and Other Catastrophes in Earth History*", **825**, 2 – 3.

Anderson, T. F., Kruger, J., Raiswell, R. (1987). C – S – F relationships and the isotopic composition of pyrite in the New Albany Shale of the Illinois Basin, U.S.A. *Geochimica et Cosmochimica Acta*, **51**, 2795 – 2805. Doi: 10.1016/0016-7037(87)90159-1

Arndt, N., Pinti, D. L. (2011). Mass Extinctions. *Encyclopedia of Astrobiologyn*, **1**, 999 – 1001. Doi: 10.1007/978-3-642-27833-4_547-3

Arthur, M. A & Sageman, B. B. (1994). Marine Shales: Depositional Mechanisms and Environments of Ancient Deposits. *Annual Review Of Earth And Planetary Sciences*, **22**, 499-551. https://articles.adsabs.harvard.edu/full/1994AREPS..22..499A/0000502.000.html

Barash, M. S. (2016). Causes of the great mass extinction of marine organisms in the Late Devonian. *Oceanology*, **56**, 863 – 875. Doi: 10.1134/S0001437016050015

Barash, M. S. (2017). Environmental Conditions as the Cause of the Great Mass Extinction of Marine Organisms in the Late Devonian. *Doklady Earth Sciences*, **475**, 845 – 848. Doi: 10.1134/S1028334X17080013

Batovrin, S., Lipovsky, B., Gulbin, Y., Pushkarev, Y., & Shukolyukov, Y. A. (2021). Constraints on the origins of iron silicide spherules in ultrahigh-temperature distal impact ejecta. *Meteoritics & Planetary Science*, ***56***(7), 1369–1405. Doi: 10.1111/maps.13662

Beier, J. A., & Hayes, J. M. (1989). Geochemical and isotopic evidence for paleoredox conditions during deposition of the Devonian-Mississippian New Albany Shale, southern Indiana. *GSA Bulletin | GeoScienceWorld*. Doi: 10.1130/0016-7606(1989)101

Bingham-Koslowski, N., Tsujita, C., Jin, J., & Azmy, K. (2016). Widespread Late Devonian marine anoxia in eastern North America: a case study of the Kettle Point Formation black shale, southwestern Ontario. *Canadian Journal of Earth Sciences*, **53**(8), 837–855. Doi: 10.1139/cjes-2015-0227

Bolton, Edward & Jr, R. & Berner, R. & Jr, J. & Petsch, S. & Mok, Ulrich & Evans, Brian. (2004). Black shale weathering: An integrated field and numerical modeling study.

Bond, D. P., & Wignall, P. B. (2008). The role of sea-level change and marine anoxia in the Frasnian–Famennian (Late Devonian) mass extinction. *Palaeogeography, Palaeoclimatology, Palaeoecology*, **263**(3–4), 107–118. Doi: 10.1016/j.palaeo.2008.02.015

Bond, D. PG. & Wignall, P. B. (2014). Large igneous provinces and mass extinctions: An update. *Volcanism, Impacts, and Mass Extinctions: Causes and Effects.* Doi: 10.1130/2014.2505(02)

Bond, D., Wignall, P. and Racki, G. (2004). Extent and duration of marine anoxia during the Frasnian – Famennian (Late Devonian) mass extinction in Poland, Germany, Austria and France. *Geological Magazine*, **141**, 173 – 193. Doi: 10.1017/S0016756804008866

Bond, D., Zaton, M., Wignall, P., and Marynowski, L. (2013). Evidence for shallow-water 'Upper Kellwasser' anoxia in the Frasnian–Famennian reefs of Alberta, Canada. *Lethaia*, **46**, 355–368. Doi: 10.1111/let.12014.

Brumsack, H. (2006). The trace metal content of recent organic carbon-rich sediments: Implications for Cretaceous black shale formation. *Palaeogeography, Palaeoclimatology, Palaeoecology*, **232**(2–4), 344–361. Doi: 10.1016/j.palaeo.2005.05.011

Campbell, G. (1946). NEW ALBANY SHALE. *GSA Bulletin*, **57**(9), 829 – 908. Doi: 10.1130/0016-7606(1946)57[829:NAS]2.0.CO;2

Chernonozhkin, S. M., De Vega, C. G., Artemieva, N., Soens, B., Belza, J., Bolea-Fernandez, E., Van Ginneken, M., Glass, B. P., Folco, L., Genge, M. J., Claeys, P., Vanhaecke, F., & Goderis, S. (2021). Isotopic evolution of planetary crusts by hypervelocity impacts evidenced by Fe in microtektites. *Nature Communications*, ***12***(1). Doi: 10.1038/s41467-021-25819-6

Chiarenza, A. A., Farnsworth, A., Mannion, P. D. *et al*. (2020). Asteroid impact, not volcanism, caused the end-Cretaceous dinosaur extinction. *Proceedings of the National Academy of Science*, **117**, 1 – 10. Doi: 10.1073/pnas.2006087117

Claeys, P., & Casier, J. (1994). Microtektite-like impact glass associated with the Frasnian-Famennian boundary mass extinction. *Earth and Planetary Science Letters*, ***122***(3–4), 303–315. Doi: 10.1016/0012-821x(94)90004-3

Claeys, P., Casier, J-G., Margolis, S. V. (1992). Microtektites and Mass Extinctions: Evidence for a Late Devonian Asteroid Impact. *Science*, **257**, 1102 – 4. Doi: 10.1126/science.257.5073.1102

Clutson, M. J., Brown, D. E., Tanner, L. H. (2018). Distal Processes and Effects of Multiple Late Triassic Terrestrial Bolide Impacts: Insights from the Norian Manicouagan Event, Northeastern Quebec, Canada. *The Late Triassic World, Topics in Geobiology*, **46**, 127 – 187. Doi: 10.1007/978-3-319-68009-5_5

Cocks, L. R. M., & Torsvik, T. H. (2011). The Palaeozoic geography of Laurentia and western Laurussia: A stable craton with mobile margins. *Earth-science Reviews*, **106**(1-2), 1 – 51. Doi: 10.1016/j.earscirev.2011.01.007

Cohen KM, Harper DA, Gibbard PL (2023) ICS International Chronostratigraphic Chart. https://www.stratigraphy.org

COLLINSON, CHARLES, L. E. BECKER, G. W. JAMES, J. W. KOENIG, and D. H. SWANN, 1967a, Illinois Basin, *in* International symposium on the Devonian System: Alberta Society of Petroleum Geologists, v. 1, p. 940-962; Illinois State Geological Survey Reprint 1968-G.

Copper, P. (2002). Reef development at the Frasnian/Famennian mass extinction boundary. *Palaeogeography, Palaeoclimatology, Palaeoecology*, **181**(1–3), 27–65. Doi: 10.1016/s0031-0182(01)00472-2

Corfu, F., Andersen, T. B., & Gasser, D. (2015). The Scandinavian Caledonides: main features, conceptual advances and critical questions. *Geological Society London Special Publications*, **390**, 9 – 43. Doi: 10.1144/SP390.25

Courtillot, V., Kravchinsky, V. A., Quidelleur, X., Renne, P. R., & Gladkochub, D. P. (2010). Preliminary dating of the Viluy traps (Eastern Siberia): Eruption at the time of Late Devonian extinction events? *Earth and Planetary Science Letters*, ***300***(3–4), 239–245. Doi: 10.1016/j.epsl.2010.09.045

Dichiarante, A. M., Langet, N., Bauer, R. A., Goertz-Allmann, B. P., Williams-Stroud, S., Kühn, D., Oye, V., Greenberg, S. E., & Dando, B. (2021). Identifying geological structures through

microseismic cluster and burst analyses complementing active seismic interpretation. *Tectonophysics*, **820**, 229107. Doi: 10.1016/j.tecto.2021.229107

Domier, M., Torsvik, T. H. (2014). Plate tectonics in the late Paleozoic. Geoscience Frontiers, **5**, 303 – 350. Doi: 10.1016/j.gsf.2014.01.002

Dunkel, C. A., Vázquez-Ortega, A., & Evans, J. E. (2022). Black shale–gray shale transitions in a Late Devonian shale succession, Central Appalachian Basin (Northern Ohio): Sedimentary and geochemical evidence for terrestrial organic matter input driving anoxia events. *Palaeogeography, Palaeoclimatology, Palaeoecology*, **608**, 111271. Doi: 10.1016/j.palaeo.2022.111271

Duverger, A., Berg, J. S., Busigny, V., Guyot, F., Bernard, S., & Miot, J. (2020). Mechanisms of pyrite formation promoted by Sulfate-Reducing bacteria in pure culture. *Frontiers in Earth Science, 8*. Doi: 10.3389/feart.2020.588310

Elewa, A. M. T., Abdelhady, A. A. (2019). Past, present, and future mass extinctions. *Journal of African Earth Sciences*, **162**, Article 103678. Doi: 10.1016/j.jafrearsci.2019.103678

Ernst, R. E., Rodygin, S. A., & Grinev, O. M. (2020). Age correlation of Large Igneous Provinces with Devonian biotic crises. *Global and Planetary Change*, ***185***, 103097. Doi: 10.1016/j.gloplacha.2019.103097

Ettensohn, F. R. & Lierman, R. T. & Mason, C. E., & Andrews, W. M., & Hendricks, R. T. & Phelps, D. J. & Gordon, L. A. (2013). The Silurian of central Kentucky, U.S.A.: Stratigraphy, palaeoenvironments and palaeoecology. *Memoirs of the Association of Australasian Palaeontologists*. **44**. 159-189. ISSN 0810-8889

Freiburg, J. T., McBride, J. H., Malone, D. H., & Leetaru, H. E. (2020). Petrology, geochronology, and geophysical characterization of Mesoproterozoic rocks in central Illinois, USA. *Geoscience Frontiers*, **11**(2), 581–596. Doi: 10.1016/j.gsf.2019.07.004

Glass, B.P., Simonson, B.M. (2012). Distal Impact Ejecta Layers: Spherules and More. *Elements* (2012), **8**(1), 43 – 48. Doi: 10.2113/gselements.8.1.43

Golonka, J. (2020). Late Devonian paleogeography in the framework of global plate tectonics. *Global and Planetary Change*, **186**, Article 103129. Doi: 10.1016/j.gloplacha.2020.103129

Golonka, J., Porebski, S. J., & Waskowska, A. (2023). Silurian paleogeography in the framework of global plate tectonics. *Palaeogeography, Palaeoclimatology, Palaeoecology*, **622**, 111597. Doi: 10.1016/j.palaeo.2023.111597

Goltrant, O., Cordier, P., & Doukhan, J. (1991). Planar deformation features in shocked quartz; a transmission electron microscopy investigation. *Earth and Planetary Science Letters*, ***106***(1–4), 103–115. Doi: 10.1016/0012-821x(91)90066-q

Hallam, A. (2022). A compound scenario for the end-Cretaceous mass extinctions. *Spanish Journal of Palaeontology*, **3**, 7 – 20. Doi: 10.7203/sjp.25155

Hammer, Ø., Jones, M. T., Schneebeli-Hermann, E., Hansen, B. B., & Bucher, H. (2019). Are Early Triassic extinction events associated with mercury anomalies? A reassessment of the Smithian/Spathian boundary extinction. *Earth-science Reviews*, ***195***, 179–190. Doi: 10.1016/j.earscirev.2019.04.016

Hasenmueller, N. R. & Woodard, G. S. (1981). Studies of the New Albany Shale (Devonian and Mississippian) and Equivalent Strata in Indiana. *State of Indiana Department of Natural Resources Geological Survey*, https://scholarworks.iu.edu/iuswrrest/api/core/bitstreams/38985409-6e65-43ec-8fe1-6c3959cacf4b/content

Hatch, J. R., & Affolter, R. H. (2002). Resource assessment of the Springfield, Herrin, Danville, and Baker coals in the Illinois Basin. *U.S. Geological Survey Professional Papers/U.S. Geological Survey Professional Paper*. Doi: 10.3133/pp1625d

Heidlauf, D. T., Hsui, A. T., & Klein, G. (1986). Tectonic Subsidence Analysis of the Illinois Basin. *The Journal of Geology*, **94**(6), 779 – 794. https://www.jstor.org/stable/30071583

Hir, G. L., Donnadieu, Y., Godderis, Y., Meyer-Berthaud, B., Ramstein, G., & Blakey, R. C. (2011). The climate change caused by the land plant invasion in the Devonian. *Earth and Planetary Science Letters*, **310**(3-4), 203 – 212. Doi: 10.1016/j.epsl.2011.08.042

Janocha, J., Wesenlund, F., Thießen, O., Grundvåg, S., Koehl, J. P., & Johannessen, E. P. (2024). Depositional environments and source rock potential of some upper palaeozoic (Devonian) coals on Bjørnøya, Western Barents shelf. *Marine and Petroleum Geology*, **163**, 106768. Doi: 10.1016/j.marpetgeo.2024.106768

Jones, M. T., et al. (2023). "Tracing North Atlantic volcanism and seaway connectivity across the Paleocene–Eocene Thermal Maximum (PETM)." *EGUsphere* **2023**: 1-53. Doi: 10.5194/egusphere-2023-36

Jutras, P., & Dostal, J. (2023). Late Ordovician to Early Devonian tectono-magmatic prequel to the Acadian Orogeny in northeastern North America and the British Isles. *Gondwana Research*, **124**, 378 – 400. Doi: 10.1016/j.gr.2023.08.002

Kabanov, P., Hauck, T. E., Gouwy, S., Grasby, S. E., & Van Der Boon, A. (2023). Oceanic anoxic events, photic-zone euxinia, and controversy of sea-level fluctuations during the Middle-Late Devonian. *Earth-science Reviews*, **241**, 104415. Doi: 10.1016/j.earscirev.2023.104415

Kaiser, S.I., Aretz, M. and Becker, R.T. (2016). The global Hangenberg Crisis (Devonian–Carboniferous transition): review of a first-order mass extinction. *Geological Society, London, Special Publication*, **423**, 355–386. Doi: 10.1144/SP423.9.

Keller, G., Sahni, A., Bajpai, S. (2009). Deccan volcanism, the KT mass extinction and dinosaurs. *Journal of Biosciences*, **34**, 709 – 728. Doi: 10.1007/s12038-009-0059-6

Kleinmann, B. (1969). Magnetite bearing spherules in tektites. *Geochimica Et Cosmochimica Acta*, ***33***(9), 1113–1120. Doi: 10.1016/0016-7037(69)90067-2

Lazar, O. R., & Schieber, J. (2022). New Albany Shale, Illinois Basin, USA—Devonian Carbonaceous Mudstone Accumulation in an Epicratonic Sea: Stratigraphic Insights from Outcrop and Subsurface Data. *Sequence stratigraphy: Applications to fine-grained rocks: AAPG Memoir*, **126**, 249–294. Doi: 10.1306/137123043860

Lazar, R., & Schieber, J. (2004). *Devonian black shales of the eastern U.S. New insights into sedimentology and stratigraphy from the subsurface and outcrops in the Illinois and Appalachian Basins: Field Guide for the 2004 Annual Field Conference of the Great Lakes Section of SEPM*. https://hdl.handle.net/2022/28825

Lin, M., Xi, K., Cao, Y., Liu, K., & Zhu, R. (2023). Periodic paleo-environment oscillation on multi-timescales in the Triassic and their significant implications for algal blooms: A case study on the lacustrine shales in Ordos Basin. *Palaeogeography, Palaeoclimatology, Palaeoecology*, **612**, 111376. Doi: 10.1016/j.palaeo.2022.111376

Lineback, J. A. (1970). Stratigraphy of the New Albany Shale in Indiana. Indiana Geological Survey Bulletin, **44**, 73 p.

Liu, B., Mastalerz, M., Schieber, J., & Teng, J. (2020). Association of uranium with macerals in marine black shales: Insights from the Upper Devonian New Albany Shale, Illinois Basin. *Internal Journal of Coal Geology*, **217**, 103351. Doi: 10.1016/j.coal.2019.103351

Lorenz, R. (2000). Microtektites on Mars: Volume and texture of distal impact ejecta deposits. *Icarus*, ***144***(2), 353–366. Doi: 10.1006/icar.1999.6303

Lyne, J., Tauber, M., Fought, R. (1996). An analytical model of the atmospheric entry of large meteors and its application to the Tunguska Event. *Journal of Geophysical Research Atmospheres*, **101**, 23207 – 23212. Doi: 10.1029/96JE02047

Marshall, C. R. (2023). Forty Years Later – The Status of the 'Big Five' Mass Extinctions. *Cambridge Prisms: Extinction*, **1**, 1 – 25. Doi: 10.1017/ext.2022.4

Mason, G. M., Caffe-Cooper, D. D. (2016). Microtektite-like glassy spherules near the Frasnian-Famennian Boundary, Late Devonian, New Albany shale, Floyd County Indiana. *Geological Society of America Abstract with Programs*, **48**, #7. Doi: 10.1130/abs/2016AM-285731

Mass extinctions. (n.d.-b). https://education.nationalgeographic.org/resource/mass-extinctions/

McBride, J. H. (1998). Understanding basement tectonics of an interior cratonic basin: southern Illinois Basin, USA. *Tectonophysics*, **293**(1–2), 1–20. Doi: 10.1016/s0040-1951(98)00081-x

McClung, W. S., Eriksson, K. A., Terry, D. O., & Cuffey, C. A. (2013). Sequence stratigraphic hierarchy of the Upper Devonian Foreknobs Formation, central Appalachian Basin, USA: Evidence for transitional greenhouse to icehouse conditions. *Palaeogeography, Palaeoclimatology, Palaeoecology*, ***387***, 104–125. Doi: 10.1016/j.palaeo.2013.07.020

McGhee Jr., G. (2001). The 'multiple impacts hypothesis' for mass extinction: a comparison of the Late Devonian and the late Eocene. *Palaeogeography, Palaeoclimatology, Palaeoecology*, **176**, 47 – 58. Doi: 10.1016/S0031-0182(01)00325-X.

McGhee, G., Racki, G. (2021). Extinction: Late Devonian Mass Extinction. *Encyclopedia of Life Sciences (eLS)*, **2**, 1 – 8. Doi: 10.1002/9780470015902.a0029301

Meinhold, G., Arslan, A., Lehnert, O., & Stampfli, G. M. (2011). Global mass wasting during the Middle Ordovician: Meteoritic trigger or plate tectonic environment?. *Gondwana Research*, **19**(2), 535 – 541. Doi: 10.1016/j.gr.2010.07.001

Mikheeva, A. O. (2022). On the impact theory of mass extinction. *Mathematical Modeling in Geophysics*, **24**, 35 – 49.

Murphy, J. B., Van Staal, C. R. & Keppie, J. (1999). Middle to late Paleozoic Acadian orogeny in the northern Appalachians: A Laramide-style plume-modified orogeny?. *Geology*, **27**(7). Doi: 10.1130/0091-7613(1999)027<0653:MTLPAO>2.3.CO;2

Ocubalidet, S. G. (2013). *CONTROLS ON ORGANIC CARBON ACCUMULATION IN THE LATE DEVONIAN NEW ALBANY SHALE, WEST-CENTRAL KENTUCKY, ILLINOIS BASIN*. OpenSIUC. https://opensiuc.lib.siu.edu/theses/1138/

Over, D. J. (2021). The Devonian – Carboniferous boundary in the United States. Paleobiodiversity and Paleoenvironments, **101**, 529 – 540. Doi: 10.1007/s12549-020-00428-1

Percival, L. M. E., Davies, J., Schaltegger, U., De Vleeschouwer, D., Da Silva, A., & Föllmi, K. B. (2018). Precisely dating the Frasnian–Famennian boundary: implications for the cause of the Late Devonian mass extinction. *Scientific Reports*, ***8***(1). Doi: 10.1038/s41598-018-27847-7

Pillans, B., Simmonds, P., Hitchcock, W., Alloway, B.V. (2012). Tektites, minitektites and microtektites from the Kalgoorlie region, Western Australia. *Conference: Australian Regolith and Clays*

Pippenger, K., Estrada, L., Jones, D. S., & Cohen, P. (2023). Appalachian Basin mercury enrichments during the Late Devonian Kellwasser Events and comparison to global records. *Palaeogeography, Palaeoclimatology, Palaeoecology*, ***627***, 111751. https://doi.org/10.1016/j.palaeo.2023.111751

Rabak, I., Langston, C. A., & Powell, C. (2011b). The Reelfoot magnetic anomaly and its relationship to the Pascola Arch and the Reelfoot fault. *Seismological Research Letters*, **82**(1), 132–140. Doi: 10.1785/gssrl.82.1.132

Racki, G. (2020). A volcanic scenario for the Frasnian–Famennian major biotic crisis and other Late Devonian global changes: More answers than questions? *Global and Planetary Change*, ***189***, 103174. Doi: 10.1016/j.gloplacha.2020.103174

Racki, G., Rakociński, M., Marynowski, L., & Wignall, P. B. (2018). Mercury enrichments and the Frasnian-Famennian biotic crisis: A volcanic trigger proved? *Geology*, ***46***(6), 543–546. Doi: 10.1130/g40233.1

Rakociński, M., Marynowski, L., Pisarzowska, A. *et al.* (2020). Volcanic related methylmercury poisoning as the possible driver of the end-Devonian Mass Extinction. *Scientific Reports*, **10**, 7344. Doi: 10.1038/s41598-020-64104-2

Ramirez, M. N., Gilleaudeau, G. J., Elrick, M. *et al*. (2023). Linking anoxia, biotic events, and basin evolution in the Late Devonian Illinois Basin, North America: A geochemical approach. *Marine and Petroleum Geology*, **158**, Article 106556. Doi: 10.1016/j.marpetgeo.2023.106556

Ricci, J., Quidelleur, X., Pavlov, V., Orlov, S., Shatsillo, A., & Courtillot, V. (2013). New 40Ar/39Ar and K–Ar ages of the Viluy traps (Eastern Siberia): Further evidence for a relationship with the Frasnian–Famennian mass extinction. *Palaeogeography, Palaeoclimatology, Palaeoecology*, ***386***, 531–540. Doi: 10.1016/j.palaeo.2013.06.020

Richardson, J. E., Melosh, J., Artemieva, N., Pierazzo, E. (2006). Impact Cratering Theory and Modeling for the Deep Impact Mission: From Mission Planning to Data Analysis. *Space Science Reviews*, **117**, 241 – 267. Doi: 10.1007/1-4020-4163-2_10

Sawłowicz, Z. (1993). Pyrite framboids and their development: a new conceptual mechanism. *Acta Diabetologica*, ***82***(1), 148–156. https://doi.org/10.1007/bf00563277

Soeder, D. J. (2018). The successful development of gas and oil resources from shales in North America. *Journal of Petroleum Science & Engineering*, **163**, 399–420. Doi: 10.1016/j.petrol.2017.12.084

Speidel, L. G., Da Silva, R. C., Beck, M., Dellwig, O., Wollschläger, J., Dittmar, T., & Seidel, M. (2024). Rivers and tidal flats as sources of dissolved organic matter and trace metals in the German Bight (North Sea). *Biogeochemistry*, ***167***(3), 225–250. Doi: 10.1007/s10533-024-01117-3

Suttle, M. D., & Genge, M. J. (2017). Diagenetically altered fossil micrometeorites suggest cosmic dust is common in the geological record. *Earth and Planetary Science Letters*, ***476***, 132–142. Doi: 10.1016/j.epsl.2017.07.052

Torsvik, T. H., & Cocks, L. R. M. (2005). Norway in space and time: A Centennial cavalcade. *Norwegian Journal of Geology*, **85**, 73 -86. ISSN 029 – 196X

Tuite, M. L., Williford, K. H., & Macko, S. A. (2019). From greenhouse to icehouse: Nitrogen biogeochemistry of an epeiric sea in the context of the oxygenation of the Late Devonian atmosphere/ocean system. *Palaeogeography, Palaeoclimatology, Palaeoecology*, ***531***, 109204. Doi: 10.1016/j.palaeo.2019.05.026

Tuttle, M. L., Breit, G. N., & Goldhaber, M. B. (2009). Weathering of the New Albany Shale, Kentucky: II. Redistribution of minor and trace elements. *Applied Geochemistry*, **24**(8), 1565–1578. Doi: 10.1016/j.apgeochem.2009.04.034

Wilkin, R. T., & Barnes, H. L. (1997). Formation processes of framboidal pyrite. *Geochimica Et Cosmochimica Acta*, **61**(2), 323–339. Doi: 10.1016/s0016-7037(96)00320-1

Wilson, R. D., Schieber, J., & Stewart, C. J. (2021). The discovery of widespread agrichnia traces in Devonian black shales of North America: another chapter in the evolving understanding of a "not so anoxic" ancient sea. *Paläontologische Zeitschrift*, **95**(4). Doi: 10.1007/s.12542-021-00599-y

Xu, R., Xiao, Z., Luo, F., Wang, Y., & Cui, J. (2023). Untrackable distal ejecta on planetary surfaces. *Nature Communications*, ***14***(1). Doi: 10.1038/s41467-023-36771-y

Zhang, F., Dahl, T. W., Lenton, T. M., Lou, G., Shen, S. Z., Algeo, T. J., Planavsky, N., Liu, J., Cui, Y., Qie, W., Romaniello, S. J., & Anbar, A. D. (2020). Extensive marine anoxia associated with

the Late Devonian Hangenberg Crisis. *Earth and Planetary Science Letters*, **533**, Article 115976. Doi: 10.1016/j.epsl.2019.115976

Zhang, J., Deng, C., Liu, W., Tang, Z., Wang, Y., Ye, T., Liang, W., & Liu, L. (2021). Mercury anomalies link to extensive volcanism across the late Devonian Frasnian–Famennian boundary in south China. *Frontiers in Earth Science*, ***9***. Doi: 10.3389/feart.2021.691827

Zhang, X., Joachimski, M. M., & Gong, Y. (2021). Late Devonian greenhouse-icehouse climate transition: New evidence from conodont δ18O thermometry in the eastern Palaeotethys (Lali section, South China). *Chemical Geology*, **581**, 120383. Doi: 10.1016/j.chemgeo.2021.120383

Zhao, J., Liang, J., Long, X., Li, J., Xiang, Q., Zhang, J., & Hao, J. (2018). Genesis and evolution of framboidal pyrite and its implications for the ore-forming process of Carlin-style gold deposits, southwestern China. *Ore Geology Reviews*, ***102***, 426–436. https://doi.org/10.1016/j.oregeorev.2018.09.022

Zheng, W., Gilleaudeau, G. J., Algeo, T. J., Zhao, Y., Song, Y., Zhang, Y., Sahoo, S. K., Anbar, A. D., Carmichael, S. K., Xie, S., Liu, C., & Chen, J. (2023). Mercury isotope evidence for recurrent photic-zone euxinia triggered by enhanced terrestrial nutrient inputs during the Late Devonian mass extinction. *Earth and Planetary Science Letters*, **613**, 118175. Doi: 10.1016/j.epsl.2023.118175

Zuchuat, V., Sleveland, A., Twitchett, R., Svensen, H., Turner, H., Augland, L., Jones, M., Hammer, Ø., Hauksson, B., Haflidason, H., Midtkandal, I., & Planke, S. (2020). A new high-resolution stratigraphic and palaeoenvironmental record spanning the End-Permian Mass Extinction and its aftermath in central Spitsbergen, Svalbard. *Palaeogeography, Palaeoclimatology, Palaeoecology*, ***554***, 109732. Doi: 10.1016/j.palaeo.2020.109732